MPS/Int. RF 65 - 9
8.7.1965

P.H. STANDLEY

THE NEW PICK-UP ELECTRODES FOR THE CPS

THE NEW PICK-UP ELECTRODES FOR THE CPS

Summary

This is a report on the considerations and calculations which led to the design of the new small pick-up stations. This new type of pick-up stations fits into the pump manifolds, frees 20 straight-sections at present occupied by the old PU stations and offers the additional advantage of a more accurate closed orbit determination.

1. Introduction

The PU stations used so far for the CPS take up the whole space in the short straight-sections between the CPS magnets. Some more straight-sections (s.s.) will have to be cleared shortly for the new acceleration units and for experimental purposes with the consequence that the already rather inaccurate beam observation would become wholly insufficient.

At higher frequencies the old PU stations showed resonances, which led to signal disturbances. In order to eliminate these, the electrodes had to be connected to the cathode follower via a low-pass filter which was rather difficult to tune. Moreover, especially at higher proton beam intensities ($\approx 10^{12}$ prot./pulse), charging effects occur which disturb the PU signal considerably.

The new PU system aims at leaving the straight-sections clear and at eliminating as far as possible the disadvantages quoted. The only space at hand for their installation was in the pump manifolds for the diffusion pumps. They are located at one side of each magnet, between the magnet coils (see Photo 1).

Whereever one side of this box is used for the connection of the diffusion pump the PU system can be installed on the opposite side through an aperture of 120 mm.

2. Electrostatic pick-up electrodes

2.1 Requirements

The proton beam passing between the two symmetrical electrodes influences the voltages U_1 et U_2 (see Fig. 1). At constant intensity the voltage difference

$$U_x = U_1 - U_2$$

must be proportional to the horizontal beam deviation x and independent of the vertical beam deviation y, i.e.

$$\left[\frac{\partial U_x}{\partial x} = \text{const} = k_1\right]_{\text{intensity=const.}}$$

and (1)

$$\frac{\partial U_x}{\partial y} = 0$$

This is required of the radial as well as of the vertical electrodes analogous to

$$U_y = U_3 - U_4 \quad \text{(Fig. 2)}$$

$$\left.\begin{aligned} &\left[\frac{\partial U_y}{\partial y} = \text{const} = k_2\right]_{\text{intensity=constant}} \\ \text{and}\quad &\frac{\partial U_y}{\partial x} = 0 \end{aligned}\right\} \quad (2)$$

Allowing for the dependence on intensity we obtain

$$U_x = I \cdot k_1 x$$
$$U_y = I \cdot k_2 y \qquad (3)$$

I = intensity

k_1, k_2 = constants

In order to find the beam co-ordinates x_1, y_1 the voltage difference must be divided by one constant and the intensity. Hence the proton beam intensity must be measured either by the 4 electrodes (Fig. 1 and Fig. 2) or with an additional fifth electrode.

As the electrodes must not be hit by the beam their cross-section must of necessity be larger than that of the vacuum chamber.

With a margin of 1 cm between electrode and chamber ellipse a maximal length of 74 mm is given for the electrode by the 120 mm diameter of the installation aperture (see Fig. 3).

If one pump manifold contained only the vertical, and the following manifold (about 6 m away) only the horizontal electrodes, the beam position according to co-ordinates x and y could only be measured with the uncertainty caused by this distance. Apart from that, a number of pump manifolds are used for housing targets so that sometimes as much as 12 or even 18 m would separate the radial and vertical measurement.

If the x and y electrodes of the old system, with cylinders cut diagonally, were to be housed in one pump manifold, only ca. 3 cm length would be available for one pair. This would entail a sensitivity 5.5 times smaller than at present.

For this reason an electrode arrangement of higher sensitivity had to be found.

2.2 Calculation of electrodes by means of conformal representation

The original idea had been to combine the radial and vertical electrodes in such a way as to form together a closed elliptical cylinder (see Fig. 4). With such an arrangement the sensitivity per given length as compared to the old system can be improved by a factor of two. This gain would approximately be the same for the ratios $\frac{U_1-U_2}{U_1+U_2}$ and $\frac{U_3-U_4}{U_3+U_4}$. In comparison with the old system this would mean a double resolution.[1] Supposing that an undisturbed radial field of the proton beam could be achieved within the measuring electrodes (see Fig. 22) : for such an elliptical cylinder arrangement the conformal representation could be applied to determine the correct separation of the electrodes provided that their potentials differ only by negligible amounts and the proton-beam field lines approach the electrodes at right angles (Fig. 5). This process is described in Appendix 1.

The separation lines for the required linearity (see equation 3) were first calculated for circular electrodes by means of the IBM 7090 computer, programme and result see Appendix 2. The result were lines in the shape of cosine form when developed on a plane which corresponds to a straight cut (see Figs. 8 a,b). After this numerical computation a mathematical proof of the cosine shape was found, which is shown in Appendix 3.

As the proof of elliptical electrodes would be much more complicated (equations (4) in Appendix 1) and would in any case only be valid for an accurate ellipse, a more general path was persued.

2.3 Linearity for electrodes with an arbitrary cross-section

In the following two electrodes with any given cross-section of their x-y plane are to be investigated.(see Fig. 11). In their x-ℓ plane they are cut linearly. Alongside of the cut they are screened by electrodes at earth potential with the same cross-section.

With a proton beam which is longer than the electrodes and moves infinitely near the border-line (x-y plane) but not touching it, the influenced signal on electrode 1 is obviously proportional to the real component of P . Thus, also the difference signal between electrode 1 and 2 is

$$\triangle Q \text{ proportional to real component P} \qquad (18)$$

However, with a proton beam moving anywhere within the incircled x-y plane (Fig. 11) a different approach has to be found.

2.3.1 Analogy between charge distribution and potential

According to Fig. 12 the charge Q in point p influences a charge on the electrode e which is thus charged up to the potential

$$U_e = \frac{Q}{C_m + \frac{C_k \cdot C}{C_k + C}} \cdot \frac{C_k}{C_k + C} = \frac{C_k \cdot Q}{CC_k + C_k C_m + CC_m} \qquad (19)$$

If In the opposite case the electrode e is charged by Q , the potential in point p is

$$U_p = \frac{Q}{C + \frac{C_k C_m}{C_k + C_m}} \cdot \frac{C_k}{C_m + C_k} = \frac{C_k \cdot Q}{CC_k + C_k C_m + CC_m} \qquad (19a)$$

i.e.

$$U_p = U_e \qquad (20)$$

Equation (20) shows that a charge Q in p produces the same potential on electrode e as the charge Q on electrode e produces in point p .

Assuming the same potentials but with opposite signs on the electrodes 1 and 2, it follows that, in order to obtain a linear charge distribution on the electrodes, the same requirements as in equation (1) are valid for potential U(x) between the electrodes :

$$\frac{\partial U(x,y)}{\partial x} = \text{const} = E$$

$$\frac{\partial U(x,y)}{\partial y} = 0 \qquad (21)$$

From equation (21) it is clear that, resultant over the length ℓ , a homogeneous field E must be produced (Fig. 13). To achieve this, the rubber membrane model can be applied (we are entitled to do this as the differential Laplace equation

$$\frac{\partial^2 U}{\partial x^2} + \frac{\partial^2 U}{\partial y^2} = 0$$

is valid for the potential in an uncharged space as well as for a thin rubber membrane).

If the electrode length ℓ were constant a potential plane would be produced, as may be seen from Fig. 14a. From this figure it also becomes clear which shape an electrode should have in order to obtain a potential with an even slope (line - ··- ·· - ·· -, Fig. 14a). Fig. 14b shows the same potential plane in profile.

(For electrodes with constant length the use of the rubber membrane model is admissible on condition that the electrode is pressed into the rubber membrane in proportion to its potential. With electrodes of uneven length every point around their edges must be inserted into the rubber in proportion to potential multiplied by its length ℓ . To explain this, one must imagine the electrodes cut up in small strips (Fig. 14b). Each strip has the potential U . If one imagines the length of each strip to be infinitely small, it is again permissible to apply the rubber membrane model to find out the potential between each strip. The sum of all these potentials shows the resultant potential distribution on Fig. 14b).

2.3.2 Proof of linearity by means of Cauchy's Integration Theorem and Green's Integration Formula

In the preceeding paragra h 2.3.1 the analogy between charge distribution and potential was proved by means of the coupling capacity C_k between beam and electrode. The value of C_k depends on the beam diameter. Hence the equivalent circuit (Fig. 12b) is only valid for a constant beam diameter. Therefore a more general proof of the mentioned analogy and its a applicability for the rubber membrane model is given in Appendix 4 . The result shows that, if a beam near the electrode edge influences a charge proportional to the co-ordinate x and independent of y , this is also valid for a beam in any point inside the electrode.

In general it can be said that, if the potential distribution between electrodes is known, the influenced charge distribution as a function of beam position is known as well.

2.4 Comparison of linearity errors in various types of electrodes

In our case, in order to prevent the incidence of primary particles the best choice for the electrode cross-section seems to be an ellipse which is 1 cm larger right around than the vacuum chamber cross-section.

With the help of descriptive geometry and a planimeter the sections cut of electrodes can be arranged in such a way that the cutting curves touch each other and that all four electrode areas are the same (see Fig. 16). The latter requirement is necessary as the sum (intensity) signal should be produced from the signals of the four electrodes. Even then the sum signal is not perfect as the four electrodes together (see Fig. 16) do not form a completely closed cylinder. The sum error is however small ($< 5\%$ for a beam which moves on an ellipse with axes of 10 and 5,0 cms). A more advantageous solution can be found, as further investigations will show.

An electrode arrangement without sum errer is shown in Fig. 17a. The point of the maximal difference error can be found immediately with the help of the rubber membrane model (Fig. 17b). At 5.5 cms distance from the centre the difference error is 5.9% and increases to 14% for the maximal displacement of 7.3 cms (see Fig. 17c).

Fig. 18a shows yet another arrangement which produces a correct sum signal but has an error in the difference signal. Here again the error distribution can easily be detected by means of the rubber membrane model.

Fig. 18c shows the radial error value at 2 points. By means of conformal representation these errors were calculated for electrodes of a circular cylindrical shape and then projected on to the ellipse.

The errors were also ascertained experimentally with the help of a shifting device (see photo 2). The sum signal was kept constant during measurements. The difference voltage was accurately measured with a digital voltmeter.

The electrode shape which was finally adopted is a compromise combining the results of Figs. 16, 17b and 18b. Its form is shown in Fig. 19. The linearity errors for the whole cross-section are displayed in Figs. 48a and 48b (mean values of several electrodes). They show that the maximal horizontal error for $|y| \leqq 2$ cm and $|x| \leqq 6{,}5$ cm is less than $\pm$ 2% . The maximal vertical error for $|x| \leqq 4$ cm and $|y| \leqq 2{,}5$ cm is about $\pm$ 6% .

It may seem that, because of its inevitable error, the new electrode configuration compares unfavourably with electrodes in the shape of diagonally cut cylinders (see Fig. 20) which when properly screened have a constant sum and exact linearity.

However, in comparison, the new electrodes according to Fig. 19 have the advantage of twice the sensitivity and resolution, which should amply justify their choice. Moreover, the error in the new electrodes is a systematic one. In the rare cases where the linearity mentioned above is not sufficient, precise values could be taken from Figs. 48a and 48b.

2.5 Effects of Electrode Coupling

For reasons of space the electrodes are installed relatively near each other. Hence a mutual influence cannot be avoided.

Fig. 21 shows the equivalent circuit for the coupling. For reasons of symmetry the partial capacities between adjacent electrodes are assumed to be equal. They are called k_{13} . The partial

capacitances between electrodes installed opposite each other are called k_{12} and k_{34} The capacities to ground of the electrodes are called k_{10}

Appendix 5 gives the calculation of the coupling effects produced by the partial capacitances between the electrodes.

Results show that neither the linearity of the difference signal nor the sum signal is influenced by the coupling (equation (36)) and (37) of Appendix 5). Coupling entails however one disadvantage: the sensitivity is diminished, for the electrode type as displayed in Fig. 19 by about 18% .

3. Signal transmission

The charge Q(x) influenced on the electrodes produces the following voltage

$$U_o = \frac{Q(x)}{C_m} \qquad (38)$$

via its capacity against mass.

Within the pump manifold with its fixed dimensions it must be possible to adjust the electrodes in order to keep their centres on the the-theoretical orbit. With conventional metal electrodes this adjustment would change the capacity to ground C_m. To avoid this the electrodes were enclosed in a mass layer of their own. At first a glass ellipse was chosen as electrode support. It was lined with a metal layer. The surrounding mass layer was extended beyond the edges of the electrode support into the interior to ensure screening of the electrodes (see Fig. 22). By such an arrangement not only does the capacity to ground of the electrodes remain constant (independent of the electrode position), also the high frequency properties improve in comparison with the all-metal electrode (self-inductance is considerably diminished) .

The electrode support chosen initially was made of glass of a thickness of 2.5 mm which produced a capacitance per electrode of $C_m = 200pF$. Later, for reasons of precision and production, porcelain of a thickness of 6 mm was preferred which, however, has an electrode capacity of no more than $C_m = 50$ pF .

3.1 Differentiation-Integration Method

The simplest way of transmitting the voltage signal coming from the electrode would be to connect it directly to a suitably terminated cable.

At frequencies below

$$f_o = \frac{1}{2\pi R_1 C_1} \tag{39}$$

C_1 = electrode capacitance

R_1 = cable termination resistance

the signal U_1 at the output is differentiated (see Fig. 23). It can be restored by subsequent integration. The main advantage of this method is that it would not require any electronic equipment in a radioactive area, a fact which would become very important with an increase of intensity. For the equivalent circuit see Fig. 23. The frequency response curve is required to be constant between f_u and f_o, falling before and after (see Fig. 24). The conditions necessary to achieve this are derived mathematically in Appendix 6. The frequency response curve as shown in logarithmic representation i in Fig. 25 results from equation (44) in Appendix 5 .

The voltage ratio for $f_u < f < f_o$ follows from :

$$\frac{U_2}{U_o} = V \frac{f_u}{f_o} \tag{47}$$

For

$$f_o = 20 \text{ MHz}$$

$$f_u = 10 \text{ kHz}$$

and

$$\frac{U_2}{U_o} = 1$$

an amplification of

$$V = \frac{f_o}{f_u} = \frac{R_i C_2}{R_1 C_1} = 2000$$

is required. The order of magnitude of C_1, C_2 and R_1 is fixed :

C_1 = 100 pF

R_1 = 75 ohms

C_2 = cannot be chosen much higher than C_2 = 300 pF because of self-resonances .

Thus

$$R_i = \frac{2000 \cdot 75 \cdot 100}{300} = 50 \text{ kohms}$$

With a simple integration circuit as shown in Fig. 26 and the values quoted in the same figure, V becomes

$$V = \frac{SR_a}{R_{iR\ddot{o}} + R_a} = 2500$$

Using these results we obtain from equation (47), Appendix 6, and from the circuit and dates of Fig. 26

$$\frac{U_2}{U_o} = V \cdot \frac{f_u}{f_o} = 1{,}25$$

This circuit was chosen for the fact that it uses the anode capacitance also as integration capacitance, with the consequence that the anode resistance can be chosen very high. This would then also mean a h..gh primary amplification.

The signals obtained by such a circuit are shown on photos 3, 4, 5 and 6. When these were taken, the integrator was placed at the end of a cable with a length of about 100 metres. The circuit has the disadvantage that, because of its high anode resistance R_a, a high supply voltage is required for adjusting the nominal working point.

In order to manage with smaller supply voltages a transistor integrator was tried. A further transistor was used as collector charge. Using this transistor integrator produced similar results.

The high amplification of the integration circuit had some bad effects caused by noise and microphony. Only at high beam intensities a sufficient signal/noise ratio was obtainable. Further disturbances were observed during the first beam cycles. At times distortions occurred at transition which were similar to those observed on the old PU stations and on the 400 MHz wide-band station. To a large extent these disturbances could have originated in the integrator or in the 120 m cable. Hence it was decided to concentrate first on the conventional method of using cathode followers as impedance transformers.

3.2 Cathode followers inside the vacuum

Existing cathode followers of the old PU stations were connected with the electrodes via relatively long lines. In order to avoid possibly disturbing resonances from these lines the valves were tentatively fixed next to the electrodes (see Photo 7). Under vacuum, for a constant temprature of the valve bulbs, the anode dissipation must not be more than about half its nominal value. Therefore the 6.5 W triode 3 A/167 M was used. Mounted in this place the valves are in a magnetic fringing field of $\hat{B} \approx 2500$ Gauss (Photo 7). Mounted in the most favourable position (see Fig. 27) their anode current changed by about 5% , As is visible on photos 8, 9, 10 and 11, the distortion at transition could not be eliminated even though electrode and grid of the cathode-follower were connected only through a 220 ohm stopper resistor. Many modifications were tried on the cathode follower (capacitive-galvanic coupling, automatic and fixed grid biasing etc.) without effect on the distortion.

Hence the disturbances did not seem to be caused by an overload of the cathode-follower due to the high frequency components at transition; they rather seemed to arrive via the electrode. With a high intensity spiralling beam mostly negative charges, and some positive ones, were observed (see Photo 12). These signal disturbances depended very considerably on the position in the ring and on time.

Due to outgassing of the valves and circuit elements the vacuum around the PU station deteriorated by a factor of 3. This method was therefore abandoned.

3.3 Cathode followers outside the vacuum

,Since there was no advantage in having the valves inside the vacuum, they were mounted outside. Here the magnet fringing field is still max. 1.5 kGauss ($\frac{\Delta I_a}{I_a} \approx 2\%$) . Electrodes and cathode-followers were connected by miniature coaxial cables ($Z = 75\Omega$).

As against the old one, only the supplementary RC filter at the entrance was omitted in the new cathode-follower circuit. Allowing for an input resistance of R_g = 500 kohms at the cathode-follower, the input time constant τ would then be only :

$$\tau = R_g C_m = 25 \mu s$$

(with C_m = 50 pF for the porcelain electrodes).

Using a cathode-follower with a compensated input divider (see Fig.28) it is possible to increase the time constant τ by the factor

$$\frac{R_s + R_g}{R_g} \qquad (48)$$

In order to keep the divider frequency independent, it is necessary that

$$R_s C_k = R_g C_E \qquad (43)$$

Thus, the input capacity is compensated and the stage can operate up to very high frequencies. During one experiment using a D 3a valve a band-width of almost 300 MHz was measured. One disadvantage of this stage is that the divider decreases the input signal by a factor of $\frac{R_g}{R_s + R_g}$. Finally, a cathode-follower circuit was chosen having a low-frequency input resistor of

$$R_i = \frac{R_g}{1-V} = \frac{R_g}{0,2} = 5 R_g$$

(V = 0,8 = amplification factor)

This circuit is shown in Fig. 29. With an electrode capacitance of C_m = 50pF and R_g = 500 kohms, the grid time constant is

$$\tau_g = 5\, R_g \cdot C_m = 125\,\mu s$$

This seems to be sufficient. The signal is attenuated only by the amplification V of the cathode-follower.

3.4 Formation of the sum signal

As mentioned before, with the new type of PU electrodes the intensity signal must be derived from all 4 individual signals taken together.

The sum is produced by a resistance network in the head amplifier. Fig. 30 shows the basic circuit diagram, Fig. 31 the equivalent circuit.

By means of the Millman Theorem the following sum signal is obtained directly :

$$U_\Sigma = (U_1 + U_2 + U_3 + U_4) \cdot \frac{R_2}{R_1+4R_2} \qquad (50)$$

for $R_1 \gg R_i$

3.4.1 Reaction on adjacent cathodes

The sum signal U_Σ reacts on each adjacent cathode with a tension (Fig. 31)

$$U_R = U_\Sigma \cdot \frac{R_i}{R_1} = \sum_1^4 U_r \cdot \frac{R_2}{R_1+4R_2} \cdot \frac{R_i}{R_1} \qquad (r = 1...4)$$

or approximately

$$U_R \approx \sum_1^4 U_r \cdot \frac{2R_2 \cdot R_i}{3R_1^2} \qquad \text{with} \qquad (4R_2 \approx \tfrac{1}{2} R_1)$$

$$U_R \approx \sum_1^4 U_r \, \frac{2}{3} \frac{R_2}{R_1^2} \cdot \frac{1}{S} \tag{51}$$

Allowing for

$$\frac{U_R}{\Sigma U} \leqq 2.5\ ^{o}/_{oo} = k$$

with equation (51)

$$R_1 \geqq \sqrt{\frac{2}{3} \frac{R_2}{Sk}} \tag{51a}$$

For R_2 = 75 ohms and S = 35 mA/V it follows that :

$$R_1 \geqq 755 \text{ ohms} .$$

The value chosen for R_1 = 820 ohms . Thus, according to equation (50) :

$$U_\Sigma = (U_1 + U_2 + U_3 + U_4) \cdot \frac{R_2}{R_1 + 4R_2}$$

$$U_\Sigma = 0{,}067 \sum_1^4 U_r \tag{52}$$

3.4.2 Lowest measurable beam intensity

Leaving aside such sources of disturbances as cavities, inflectors etc. the smallest still detectable beam intensity value is determined by the S/N ratio. Calculation must be done at the input of the sum amplifier as here the signals are smallest. According to equation (33), Appendix 5, the sum voltage of the 4 electrodes is :

$$U_1 + U_2 + U_3 + U_4 = \frac{\Sigma Q}{C_m} = U_S \qquad (53)$$

($C_m = k_{10} = 50$ pF = electrode capacitance)

with

$$\Sigma Q = \frac{P \cdot e \cdot \ell}{L} \qquad (54)$$

(bunching factor not considered)

L = ring circumference
= 628 m

P = Prot/pulse

e = $1{,}6 \cdot 10^{-19}$ AS

ℓ = electrode length
= 6 cm

According to equs. (53) and (54)

$$U_S = \frac{P \cdot e \cdot \ell}{C_m L} \qquad (55)$$

Amplification of the cathode followers is V = 0,8 . As a result, the following value is obtained at the output of the sum network (see equation 52) :

$$U_\Sigma = V\, U_S \cdot 0{,}067 = 0{,}8 \cdot \frac{P \cdot e \cdot \ell}{C_m L} \cdot 0{,}067 \qquad (56)$$

Two main noise sources exist here : $R_2 = 75$ in series with the equivalent noise resistance R_{eq} of the first step of the sum amplifier (see Fig. 31).

$$R_N = R_{eq} + R_2$$

Thus, the noise voltage is :

$$U_N = \sqrt{4k\ T\ \Delta f\ R_N} = 0{,}126 \sqrt{R_N [k\Omega]\ \Delta f\ [kHz]} \quad [\mu V]$$

With

$R_N = 400$ ohms

$\Delta f = 30$ MHz

$$U_N = 0{,}126 \sqrt{0{,}4 \cdot 30000} = 14 \mu V$$

Assuming a S/N ratio of $\frac{U_\Sigma}{U_N} = 2$ combined with equ. (56), the minimum beam intensity value is :

$$P_{min} = \frac{2U_N \cdot C_m L}{e \cdot \ell \cdot 0{,}067 \cdot 0{,}8}$$

$$P_{min} = 1{,}7 \cdot 10^9 \text{ Prot/pulse} \quad .$$

4. Disturbance sources within the PU stations and their elimination

Several test PU stations with the new electrode arrangement (see Photo 13) were constructed and mounted in the machine. Signals obtained with these new stations showed disturbances of various kinds. Mainly, a negative deviation of the base line was observed at injection and transition.

4.1 Influence of the grid current

Some PU stations showed a peculiar slumping of their base line (see Photo 14). The assumption was that the accumulative disturbance occuring at double synchrotron frequency was caused by the grid current in the cathode-follower tube. Examination of these D 3a tubes revealed that the grid current was 0,1 μA at a grid voltage of -1,5 V. Thes effect disappeared, however, after the working point of the tube had been displaced further into the negative range.

4.2 Influence of the non-linear characteristic of the cathode-follower tubes

Appendix 7 contains an approximate derivation of what happens when a modulated signal at transition is transmitted by a cathode-follower with a non-linear characteristic.

It was found that a supplementary modulation m^* with the double synchrotron frequency Ω occurs :

$$m^* = mk \tfrac{1}{2} \frac{T^2}{S} U_m^2 \cdot \frac{Z_k}{(1+SZ_k)^2} \qquad (65)$$

with Z_k = cathode impedance $R_K \| C_p$

U_m = carrier amplitude of the fundamental (s. Fig. 34)

S = Mutual conductance

T = Curvature in the working point

k,m = Constants .

It can be seen from equation (65) that the modulation factor m^* is proportional to the square of the curvature T and inversely proportional to the mutual conductance S .

As in general the curvature T decreases with increasing mutual conductance, operating with a high anode current is an advantage. A limit is set however by the grid current and the maximal power dissipation.

4.3 Resonances of the electrodes and their connecting lines

At transition the amplitude of the synchrotron oscillations becomes very much larger, i.e. bunches become very short and produce pulses of a few nanoseconds' length. The harmonics of these pulses are apt to excite resonances on the electrode and its supply lines. Thus, the enhanced amplitudes of the harmonics might cause an overdrive at the cathode-follower input.

Frequency analysis of a pulse of 2 ns and a 10 MHz repetition frequency revealed that the 20th harmonic still has 65% of the fundamental amplitude.[8] At high frequencies resonances could equally be excited by incident particles.

Appendix 8 contains a graphic and mathematical investigation as to which amplitudes were caused by the higher harmonics at the end of the transmission line (before the cathode-follower input). The maximal amplitude of harmonics up to f = 600 MHz was found to be less than 3 times the value of the low frequencies.

In order to damp more efficiently the resonances on the electrodes the porcelain support was covered with a layer of antimony (replacing the silver) which served as surface resistance. Its specific value was

$$R^* \approx 5 \text{ ohms}$$

This did not remove the signal disturbances, which shows that the electrode resonances are of minor importance among the causes for these disturbances. This is also corroborated by the fact that electrodes with cathode-followers attached to them in the vacuum (i.e. without cables) did not eliminate the disturbances.

4.4 Influence of the residual gas ions and secondary electrons

At injection the base line frequently showed a stronger deviation than could be accounted for by the R.C. grid time constant of the cathode-follower.

These indications of a recharging process seemed to be caused by electrons hitting the electrodes. To confirm this, the electrode was biased (with respect to the chamber) with a negative voltage which was supposed to ward off low-energy negative particles. As can be seen on photos 15 and 16, this was possible with $V = -50$ V. Increasing the negative voltage still further provoked a positive charge on the electrode (photo 17), ie. positive ions were attracted. The bias voltage necessary to obtain an undisturbed signal was not constant but depended on where the station was placed in the ring, also, it varied from time to time of measuring.

From photos 15 and 16 (signals of the radial electrode) it becomes obvious that the negative slump of the base line occurs mainly when the beam is extremely displaced. In this case many protons hit the vacuum chamber wall and hence the supposition is that the negative charge is caused by secondary electrons produced at the vacuum-chamber wall (and having a high secondary emission factor of the small incident angles).

At transition, also the protons are extremely displaced transversally. Here, too, part of the distortion could be eliminated by a negative bias-voltage (see photos 18 and 19). Unfortunately this could not be achieved in a reproducible way. In order to

prevent charged particles of low energy from settling on the electrode the latter would have to be biassed corresponding to the energy of the incident particles. This can be achieved with an automatic biasing mechanism.

If the electrode is protected by a dielectric layer, charged particles will land on the electrode until the counter potential $U_{counter}$ corresponds to the maximum energy of incident particles. This counter potential is reached the more quickly the smaller the capacitance between dielectric layer and electrode.

At injection, four of five stations no longer showed signs of charging-up after their electrodes had been protected by a Teflon layer. Only the base line of the fifth station showed a negative deviation after 20 beam revolutions. This may have been due to particles of higher energies which did not charge up the Teflon layer but passed through it.

At transition, the protective Teflon layer had no influence on the charging-up effect. This effect also remained unchanged when the H.F. signal influenced on the electrodes was suppressed by a low-pass filter (f_c = 500 kHz) between electrode and cathode-follower. Increasing the pressure of the vacuum by a factor of 10 was of no consequence either.

The frequency of the charging-up voltage is relatively low. A 12 kHz high-pass filter at the cathode-follower output suffices to obtain PU signals which are almost completely without disturbances.

Summing up, it may be said that it proved possible, by appropriate counter-measures, to eliminate disturbances of high frequencies originating from electrodes and supply-line resonances, or from the cathode-followers. To eliminate signal disturbances of low frequencies caused by incident charged particles of high energy or γ-radiation, a filter is required.

5. Construction

Fig. 47 explains the construction of the new PU stations. An appropriate moving mechanism will ensure that the measuring electrodes in the vacuum may be adjusted according to the theoretical beam orbit.

For adjustment, a measuring telescope serves as reference, with a mark oriented towards a measuring point on each of the 2 adjacent magnet units.

The cathode followers with their sum network for signal transmission described above can be plugged in, i.e. they are easily exchangeable. The plug-in unit is fitted with a test input. From here a test signal can be coupled capacitively, via 2 relays, with the cathode-follower inputs on each of the four cathode-follower grids.

It is also possible to plug in only four cables instead of the cathode-followers. In that case the transmitted signal must be regenerated by the method described in paragraph 4.1 . This would have the advantage of no electronics in a radio-active area.

Photo 20 shows the prototype in its final shape. On photos 21, 22, 23 sum signals received by the prototype electrode can be seen.

In a later report the ensuing quotient formation from difference and sum signal $(\frac{\Delta}{\Sigma})$ as mentioned in paragraph 2.1 will be described.

G. Schneider

ACKNOWLEDGMENTS

I wish to express my gratitude to Mr. H. Fischer for suggesting this interesting work to me, for his continuous interest, encouragement and advice.

It is a pleasure to acknowledge the stimulating discussions held with Drs. H.G.Hereward, A.A. Kuzmin, and with Messrs. H.Isch, K.Gase and H.-H. Umstätter.

I am further indebted to Mr. P. Opitz and Mr. J.M.Baillod for their valuable practical help.

To Mr. W. Wünsche I owe thanks for the mechanical construction, and to Mr. P. Bigler for some of the drawings contained in this report.

6. REFERENCES

1. K. Gase : Difference Amplifier for the Beam Observation System, MPS/Int RF 64-9

2. H. Kober : Dictionary of Conformal Representations, USA, 1957

3. Bronstein-Semendjajew: Taschenbuch der Mathematik, Leipzig 1959, p. 323

4. " " : Taschenbuch der Mathematik, Leipzig 1959, p. 320

5. K. Simonyi : Theoretische Elektrotechnik, Berlin 1956, p. 226

6. " : Theoretische Elektrotechnik, Berlin 1956, p. 143

7. Dr. H. Schröder : Elektrische Nachrichtentechnik, Bd. I Berlin 1959, p. 437

8. R.K. Kaiser : Analysis of PU Electrode Signal, MPS/Int RF 64 - 5

9. Meinke-Gundlach : Taschenbuch der Hochfrequenztechnik, Berlin, Göttingen, Heidelberg, 1962, p. 260

Distribution : (open)

MPS Scientific and Technical Staff

APPENDIX 1

Calculation of the electrode shape ba conformal representation

The transformation steps from the z via the t to the w-plane are represented in Fig. 6. The function from z to t is

$$t = \sqrt{k}\, sn\left(\frac{2K}{\pi} \sin^{-1} \frac{z}{\sqrt{a^2 - b^2}}\right) \tag{4}$$

with

$$K = \int_0^{\pi/2} \frac{d\varphi}{\sqrt{1 - k^2 \sin^2 \varphi}}$$

$$k = \left(\frac{\Theta_2^2(\tau)}{\Theta_3^2(\tau)}\right)^2 ; \qquad e^{i\pi\tau} = \left(\frac{a-b}{a+b}\right)^2$$

$$\tau = \frac{2i}{\pi} \lg \frac{a+b}{a-b} \qquad \text{(see ref.[2])} \tag{5}$$

If the ellipse circumference is divided up into 4 n equal arc elements δ_z in the z-plane, the transformed circumference sections δ_w appear on the w-plane as arcs of the angle $\Delta\psi_\nu$ (z and w-plane, Fig. 6). Thus, that fraction of the field-lines emanating from the proton beam P is obtained which hits the arc element δ_z. By multiplying each $\Delta\psi_\nu$ (for a given position P) by an unknown length ℓ_ν and then adding up these products obtained for the individual electrodes, the difference signal for the respective proton beam position P is obtained as the difference of these terms for 2 opposite electrodes. With k = n different positions of P the n unknown lengths ℓ_ν can be determined.

The formulation for horizontal electrodes (see Fig. 7) is :

Influenced charge on electrode 1 :

$$Q_{1k} = \sum_{1}^{n} \Delta\psi_\nu \, \ell_\nu + \sum_{3n+1}^{4n} \Delta\psi_\nu \, \ell_\nu$$

Influenced charge on electrode 2 :

$$Q_{2k} = \sum_{n+1}^{3n} \Delta\psi_\nu \, \ell_\nu \qquad (6)$$

with $\ell_\nu = \ell_{2n-\nu}$ for $2n \geq \nu \geq n$

and $\ell_\nu = \ell_{\nu-2n}$ for $3n \geq \nu \geq 2n$

and $\ell_\nu = \ell_{4n-\nu}$ for $4n \geq \nu \geq 3n$

for reasons of symmetry.

Condition of linearity :

$$\Delta Q_k = Q_{1k} - Q_{2k} = \alpha \, \mathrm{Re}\,(P_k) \qquad (7)$$

or

$$\sum_{1}^{n} \Delta\psi_\nu \, \ell_\nu + \sum_{n+1}^{4n} \Delta\psi_\nu \ell_\nu - \sum_{n+1}^{3n} \Delta\psi_\nu \ell_\nu = \alpha \, \mathrm{Re}(P_K) \qquad (8)$$

As α is yet another unknown factor, a value has to be assumed in order to avoid a homogeneous system of equations. $(n-1)$ ℓ_ν values as well as the sensitivity α can be calculated with n beam positions P .

First of all the curve form of a circular cylinder electrode was calculated with the help of the IBM 7090 computer (see machine programme in Appendix 2).

The transformation function is :

$$w = \frac{Z - P}{1 - Z\bar{P}} \quad ;$$

and

$$\Delta\psi = \text{arc tg} \frac{\text{Im}(w)}{\text{Re}(w)} \qquad (5)$$

The circumference was divided up into 40 sections, corresponding to $n = 10$. Developed on a plane, the solution showed a cosine-shaped boundary (deviation ca. 1%) of the electrodes. This cosine-shaped boundary corresponds to a straight cut in the projection on the $x - \ell$ plane (see Figs. 8a, 8b).

APPENDIX 2

PICK-UP ELECTRODE PROGRAMME

```
      COMPLEX Z,S (100), W
      DIMENSION S1(100,2), DPSI(1000)
      EQUIVALENCE  (S,S1)
      DIMENSION D(1000), R(200), DT(1000), RT(200)

C     BEAM POSITION
      S(1)  = (.2,.0)
      S(2)  = (.5,.0)
      S(3)  = (.7,.0)
      S(4)  = (.3,.25)
      S(5)  = (.5,.25)
      S(6)  = (.2,.5)
      S(7)  = (.4,.5)
      S(8)  = (.3,.7)
      S(9)  = (0.05,.3)
      S(10) = (.2,.7)

      NT    = 6
      M     = 10
      MR    = M-1

      N     = M
      M0    = 1
      M1    = M+1
      M2    = 2*M+1
      M3    = 3*M+1
      M4    = 4*M+1
      MA    = M4-1
      MB    = M4*2
      MC    = MA/2
      DELTA = 3.1415926/FLOAT(MC)
      JK    = 0

      DO30 K= 1,N

      PHI   = -DELTA

      DO 11I= 1,MB

      PHI   = PHI+DELTA
      Z     = CMPLX(COS(PHI),SIN(PHI))
      W     = (Z-S(K))/((1.,0.)-CONJG(S(K))*Z)
   11 DPSI (I) = AMAN2(AIMAG(W),REAL(W))

      DC14 I   = 1,MB
      DPSI (I) = DPSI(I+1)-DPSI(I)
  113 IF (DPSI(I)) 213,14,14
  213 DPSI(I)  = DPSI(I)+6.2831852
   14 CCNTINUE
      WRITE (NT,12)K,S(K),(DPSI(I),I=1.M4)
```

```
   12 FORMAT (////X14/X2F10.2//(X10F10.6))

   DO 15 I = 2,M
   I1      = M2+I-1
   I2      = M2-I
   I3      = M4-I

   J       = JK+I-1
15 D(J)    = (DPSI(I)-DPSI(I1))-(DPSI(I2)-DPSI(I3))

   D(J+1)  = -REAL(S(K))
   R(K)    = (DPSI(M2)-DPSI(1))+(DPSI(M2-1)-DPSI(M4-1))

30 JK      = JK+N

   CALL MXTRP (D,DT,N,N,)
   CALL MXEQU (D,R,N,1)

   WRITE (NT,32)(R(I),I = 1,N)

   32 FORMAT (////6HO***** 10F10.5/(6X10F10.5))
   32 FORMAT (////9HO RESULT..//(6X10F10.5))

   RETURN
    END
```

```
   RESULT
   0.98078
   0.92066
   0.86536
   0.75448
   0.66111
   0.51681
   0.39146
   0.22634
   0.08920
   6.30405
```

APPENDIX 3

Proof of linearity of linearly cut, circular cylinder electrodes

If it can be shown that the difference of the charges influenced by a beam P on the electrodes 1 and 2 (see Fig. 9) is proportional only to the real part of point P , this would prove the linearity of the electrode with the length

$$\ell_{(\varphi)} = \cos \varphi$$

In other words

$$\int_0^{2\pi} \ell\ (\varphi)\ d\psi \overset{?}{\text{ prop Re P}} = r \cos \chi \tag{12}$$

or

$$I = \int_0^{2\pi} \ell\ (\varphi)\ \frac{d\psi}{d\varphi}\ d\varphi \overset{?}{\text{ prop r}} \cos \chi \tag{13}$$

φ can be integrated from 0 till 2π , as the difference between the charges of electrodes 1 and 2 is caused by $\cos \varphi$ (the latter being negative in the second and third quadrant.

It is

$$\frac{d\ \psi}{d\ \varphi} = \left| \frac{d\ w}{d\varphi} \right| \tag{14}$$

as the unit circle in the z-plane is projected on to the unit circle in the w-plane (see Fig. 9) .

From equation (5)

$$\frac{d\psi}{d\varphi} = \left|\frac{dw}{d\varphi}\right| = \left| \frac{ie^{i\varphi} - r^2 ie^{i\varphi}}{(1 - re^{i(\varphi-\chi)})^2} \right|$$

$$\frac{d\psi}{d\varphi} = \frac{(1 - r^2)}{(1 - r\cos(\varphi-\chi))^2 + (r\sin(\varphi-\chi))^2}$$

$$\frac{d\psi}{d\varphi} = \frac{1 - r^2}{1 + r^2 - 2r\cos(\varphi-\chi)} \qquad (15)$$

With this it follows for the integral I (equation (13)) that

$$I = \int_0^{2\pi} \frac{(1 - r^2)\cos\varphi d\varphi}{1 + r^2 - 2r\cos(\varphi-\chi)}$$

$\xi = \varphi - \chi$ substituted leads to

$$I = (1 - r^2) \int_{-\chi}^{2\pi-\chi} \frac{\cos(\xi + \chi)\, d\xi}{1 + r^2 - 2r\cos\xi}$$

$$I = (1 - r^2) \int_{-\chi}^{2\pi-\chi} \frac{\cos\chi\cos\xi\, d\xi}{1 + r^2 - 2r\cos\xi} - (1 - r^2) \int_{-\chi}^{2\pi-\chi} \frac{\sin\chi\sin\xi d\xi}{1 + r^2 - 2r\cos\xi}$$

$$I = I_1 - I_2$$

From [3] integral I_2 can be found :

$$I_2 = \frac{(1-r^2)}{2r} \sin\chi \ln (1+r^2 - 2r\cos\xi) \Big|_{\xi=-\chi}^{2\pi-\chi} = 0 \qquad (16)$$

From [4] :

$$I_1 = (1-r^2)\cos\chi \left\{ \frac{\xi}{-2r} + \frac{1+r^2}{2r} \cdot \frac{2}{\sqrt{(1+r^2)^2-4r^2}} \operatorname{arctg} \frac{(1+r^2+2r)\operatorname{tg}\xi/2}{\sqrt{(1+r^2)^2-4r}} \right\} \Big|_{\xi=-\chi}^{2\pi-\chi}$$

$$I_1 = \left(-\frac{2\pi}{2r} + \frac{1+r^2}{1-r^2}\frac{2\pi}{2r}\right) (1-r^2)\cos\chi$$

$$I_1 = 2\pi r \cos\chi$$

Therefore also :

$$I \text{ prop. } r\cos\chi$$

q. e. d.

APPENDIX 4

Proof of linearity of linearly cut, cylindrical electrodes with arbitrary cross-section

In Fig. 15 an arbitrary shape of electrode is shown with the co-ordinates $\zeta = \xi + j\eta$ on the edge. If the proton beam moves on the edge (infinitely near but not touching the electrodes) it influences a charge

$$Q = C\,\xi \quad . \tag{22}$$

for linearly cut electrodes in the x-ℓ plane (see Fig. 15). $Q = C\,\xi$ is the real part of the complex analytical function :

$$f(\zeta) = C\,\zeta = C\,\xi + jC\eta = Q + jP \tag{23}$$

With the help of the Cauchy Integral Theorem

$$f(z) = \frac{1}{2\pi\,j} \oint \frac{f(\zeta)\,d\zeta}{\zeta - z} \tag{24}$$

it is possible to determine a regular function $f(z)$, if the function $f(\zeta)$ is known for all points around the edge. Adding the imaginary component $jP = jC\eta$ is permissible on the grounds that either real or imaginary part of an analytical function fulfils the Laplace differential equation [5] . Determined by the integral theorem (equation (24)) the function $f(z)$ within the encircled area is obtained by changing ζ with z in the function $f(\zeta)$.

Therefore :

$$f(z) = C\,z = Cx + j\,C\,y \tag{25}$$

Thus also

$$Q = C\,X \tag{26}$$

is valid within the area of the real part.

A direct relation between the real part Q of a complex analytical function $f(z) = Q(x,y) + jP(x,y)$ and a function $f(\zeta) = Q(\xi, \eta)$ (known for all points around the edge of the electrodes) is indicated by Greens formula

$$Q(x,y) = \frac{1}{2\pi} \oint Q(\xi,\eta) \frac{\partial g}{\partial n}\, ds \tag{27}$$

$$g = -\ln |\varphi(\xi,z)| = \text{Green's function}$$

where

$$\frac{\partial g}{\partial n} \cdot ds = \frac{1}{j} \frac{\varphi'(\zeta,z)}{\varphi(\zeta,z)}\, d\zeta$$

with $w = \varphi(\zeta,z)$, a transformation function, which maps point z in point 0 of the w-plane and point ζ of the limiting curve on the unit circle of the w-plane. This always holds good, according to Riemann's Fundamental Theorem valid for any simple coherent area with at least 2 points on the edge.

These theorems and considerations go to show that

$$Q = C\,X \tag{26}$$

is as valid within the area as

$$Q = C\xi$$

on the edge. For the case discussed here this means that the difference charge influenced on the electrodes by the proton beam (everywhere between the electrodes) is proportional to one co-ordinate , provided this holds also for a beam positi n around the edge of the electrode .

APPENDIX 5

Electrode coupling

Assuming that $Q_\nu (\nu = 1 \div 4)$ are the charges on the 4 electrodes 1 ÷ 4 (see Fig. 21), and U_ν the respective potentials, it follows according to Maxwell that

$$
\begin{aligned}
Q_1 &= U_1 k_{10} + (U_1 - U_2)\, k_{12} + (U_1 - U_3) k_{13} + (U_1 - U_4)\, k_{13} \\
Q_2 &= U_2 k_{10} + (U_2 - U_1)\, k_{12} + (U_2 - U_3) k_{13} + (U_2 - U_4)\, k_{13} \\
Q_3 &= U_3 k_{10} + (U_3 - U_4)\, k_{13} + (U_3 - U_4) k_{34} + (U_3 - U_1)\, k_{13} \\
Q_4 &= U_4 k_{10} + (U_4 - U_1)\, k_{13} + (U_4 - U_2) k_{13} + (U_4 - U_3)\, k_{34}
\end{aligned}
\tag{28}
$$

or, rearranged :

$$
\begin{aligned}
Q_1 &= U_1 (k_{10} + k_{12} + 2k_{13}) - U_2 k_{12} - U_3 k_{13} - U_4 k_{13} \\
Q_2 &= U_2 (k_{10} + k_{12} + 2k_{13}) - U_1 k_{12} - U_3 k_{13} - U_4 k_{13} \\
Q_3 &= U_3 (k_{10} + k_{34} + 2k_{13}) - U_1 k_{13} - U_2 k_{13} - U_4 k_{34} \\
Q_4 &= U_4 (k_{10} + k_{34} + 2k_{13}) - U_1 k_{13} - U_2 k_{13} - U_3 k_{34}
\end{aligned}
\tag{29}
$$

The difference between the charges of two opposite electrodes is :

$$\begin{aligned} Q_1 - Q_2 &= (U_1 - U_2)\,(k_{10} + 2k_{12} + 2k_{13}) \\ Q_3 - Q_4 &= (U_3 - U_4)\,(k_{10} + 2k_{34} + 2k_{13}) \end{aligned} \tag{30}$$

and the sum :

$$Q_1 + Q_2 + Q_3 + Q_4 = (U_1 + U_2 + U_3 + U_4)\,k_{10} \tag{31}$$

Hence :

$$\begin{aligned} U_1 - U_2 &= \frac{Q_1 - Q_2}{k_{10} + 2k_{12} + 2k_{13}} \\ U_3 - U_4 &= \frac{Q_3 - Q_4}{k_{10} + 2k_{34} + 2k_{13}} \end{aligned} \tag{32}$$

$$U_1 + U_2 + U_3 + U_4 = \frac{Q_1 + Q_2 + Q_3 + Q_4}{k_{10}} \tag{33}$$

Without coupling capacitors one had

$$\begin{aligned} U_1' - U_2' &= \frac{Q_1 - Q_2}{k_{10}} \\ U_3' - U_4' &= \frac{Q_3 - Q_4}{k_{10}} \end{aligned} \tag{34}$$

$$U_1' + U_2' + U_3' + U_4' = \frac{Q_1 + Q_2 + Q_3 + Q_4}{k_{10}} \tag{35}$$

and for the quotients :

$$\frac{U_1 - U_2}{\Sigma U} = \frac{U_1' - U_2'}{\Sigma U'} \cdot \frac{1}{1 + \frac{2k_{12}}{k_{10}} + \frac{2k_{13}}{k_{10}}}$$

$$\frac{U_3 - U_4}{\Sigma U} = \frac{U_3' - U_4'}{\Sigma U'} \cdot \frac{1}{1 + \frac{2k_{34}}{k_{10}} + \frac{2k_{13}}{k_{10}}} \qquad (37)$$

This makes it clear that the sensitivity of the difference signal as well as of the quotient signal is decreased by a constant factor. As the calculations show, neither the sum signal nor the electrode linearity is influenced by the coupling capacitors.

On an electrode laid out according to Fig. 19, with a disconnecting strip of 2,5 mm, the values k_{13}, k_{12}, k_{34}, k_{10} were measured.

$$k_{10} = 50 \text{ pF}$$

$$k_{12} \sim k_{34} \sim 0{,}5 \text{ pF}$$

$$k_{13} = 5 \text{ pF}$$

Owing to the coupling effect the decrease in sensitivity in vertical as well as radial direction, worked out on the basis of the above values, is :

$$1 - \frac{1}{1 + 2 \cdot 0{,}01 + 2 \cdot 0{,}1} \sim 18\%$$

APPENDIX 6

Mathematical part of the differentiation - integration method

The conclusions to be drawn from Fig. 23 are :

$$\frac{U_1}{U_o} = \frac{R_1}{R_1 + \frac{1}{pC_1}} \quad ; \quad (p = j\omega) \tag{40}$$

$$\frac{U_1}{U_o} = \frac{pC_1R_1}{1 + pC_1R_1} \tag{41}$$

$$\frac{U_2}{VU_1} = \frac{\frac{1}{pC_2}}{R_i + \frac{1}{pC_2}} \tag{42}$$

$$\frac{U_2}{VU_1} = \frac{1}{1 + pC_2R_i} \tag{43}$$

$$\frac{U_2}{U_o} = \frac{U_2}{VU_1} \cdot \frac{U_1}{U_o} \cdot V = \frac{1}{(1 + pC_2R_i)} \cdot \frac{pC_1R_1}{(1 + pC_1R_1)} \cdot V \tag{44}$$

Within a certain frequency range there are 2 possibilities of making $\frac{U_2}{U_o}$ independent of the frequency :

a) and $\alpha.)$ $|pC_1R_1| \gg 1$ and $\beta.)$ $|pC_2R_i| \ll 1$ (45) this leads to $\frac{U_2}{U_o} = V$ (45a)

Condition α is impossible to realise owing to the low cable characteristic impedance and the small capacity of the electrodes.

b) and $\alpha.)\ |pC_1R_1| \ll 1$ $\beta.)\ |pC_2R_i| \gg 1$ (46) this leads to $\frac{U_2}{U_o} = V \cdot \frac{C_1R_1}{C_2R_i}$ (46a)

Condition $\alpha.)$ must be met up to frequency $f_o = \frac{1}{2\pi R_1 C_1}$

Condition $\beta.)$ must be met down to frequency $f_u = \frac{1}{2\pi R_i C_2}$ (see Fig. 24)

Thus it follows that

$$\frac{U_2}{U_o} = V \cdot \frac{f_u}{f_o} \tag{47}$$

In Fig. 25 equation (44) is plotted with logarithmic co-ordinates, showing clearly how the differentiation is compensated by the integration within the frequency limits.

APPENDIX 7

Modulation by the non-linear characteristic of the cathode-follower

Shortly after transition the synchrotron frequency is very small, from then on it increases slowly. The time interval $T = \frac{2\pi}{\Omega}$ corresponds to twice the synchrotron frequency, see Fig. 32. Since the synchrotron frequency is changing continuously, the frequency spectre of the whole cycle becomes rather complicated.

Considdring that disturbances occur around transition and immediately after owing to double synchrotron frequency, this range will be examined here on the assumption that the time interval T is more or less constant (see Fig. 33).

$$\frac{T}{\tau} = \frac{\omega}{\Omega} = n > 1 \quad \text{(whole number is assumed)}$$

The pulses below the envelop (Fig. 33) have the same area F (on account of the fixed charge of the proton bunches). At the beginning and at the end of each time interval T the pulse width is very small,and, as a consequence, the pulse very high. For this simplified pulse train the harmonic analysis is

$$U(t) = \frac{A_o}{2} + A_1 \cos \Omega t + A_2 \cos 2\Omega t + A_3 \cos 3\Omega t + \ldots. \qquad (57)$$

with

$$A_K = \frac{2}{T} \int_o^T U(t) \cos K\Omega t \, dt \qquad (K = 1, 2, 3, \ldots)$$

In case of $1 < K << \frac{T}{\tau}$

$$A_K = 0$$

Hence the spectrum has the shape as shown in Fig. 34.

On a non-linear element such a mixture of frequencies produces new frequencies, among them the frequency Ω .

Replacing the characteristic of the cathode-follower tube at the operating point by a series expansion up to the quadratic term, then

$$i_a = I_{ao} + SU_g + 1/2\ T\ U_g^2 \qquad \text{with} \quad S = \frac{\partial ia}{\partial U_g} \qquad (58)$$

$$T = \frac{\partial^2 ia}{\partial U_g^2}$$

The frequencies ω , $\omega+\Omega$ and $\omega-\Omega$, considered by themselves correspond to a sinusoidal, amplitude-modulated carrier frequency. According to ref [7] and Fig. 35 the latter, demodulated on a non-linear characteristic given by equation (58) produces a current with the frequency Ω

$$i_{a\Omega} = \frac{1}{2}\ T\ \frac{U_m^2}{(1+ SZ_K)^2}\ m \cos \Omega t \qquad (60)$$

The rectified current is

$$i_{ao} = \frac{1}{4}\ T\ U_m^2\ (1+ \frac{m^2}{2}) \cdot \frac{1}{(1+ SZ_K)^2}$$

when U_m = amplitude of carrier frequency ω (see Fig. 34)

m = modulation depth

Taking into account the higher harmonics 2ω, 3ω, .. etc. which, by demodulation, deliver the same frequency Ω, with a factor of $k > 1$, then

$$i_{a\Omega} = k \cdot \frac{1}{2} T \frac{U_m^2}{(1+ SZ_K)^2} \cdot m \cos \Omega \qquad (61)$$

$$i_{a\Omega} = P \cos \Omega t$$

where

$$P = k \cdot \frac{1}{2} T \frac{U_m^2}{(1+ SZ_K)^2} \cdot m$$

The voltage

$$i_{a\Omega} \cdot Z_K = P \cdot Z_K \cos \Omega t$$

is superimposed on the input voltage the main components of which have the frequencies ω, 2ω, 3ω, ... etc. Hence

$$U_g = \frac{1}{1+SZ_K} (A_1 \cos \omega t + A_2 \cos 2\omega t + A_3 \cos 3\omega t + ..) - PZ_K \cos \Omega t \qquad (62)$$

With this voltage the following current - among others - is produced at the tube characteristic :

$$i_a = \frac{A_1}{1+ SZ_K} (S - \frac{1}{2} kT^2 U_m^2 \frac{Z_K}{(1+ SZ_K)^2} m\cos \Omega t) \cos \omega t \qquad (63)$$

$$+ \frac{A_2}{1+SZ_K} (S - \frac{1}{2} kT^2 U_m^2 \frac{Z_K}{(1+ SZ_K)^2} m\cos \Omega t) \cos 2\omega t$$

$$+ ....$$

The output voltage of the main component is

$$U_2 = \frac{SZ_K}{1+ SZ_K} (1- m^* \cos \Omega t) (A_1 \cos \omega t + A_2 \cos 2\omega t + A_3 \cos 3\omega t) + \ldots \quad (64)$$

with

$$m^* = m \cdot k \cdot \frac{1}{2} T^2 \frac{Um^2}{S} \cdot \frac{Z_K}{(1+ SZ_K)^2} \quad (65)$$

APPENDIX 8

Resonances of Electrodes

In the following the possible signal distortion caused by resonances from the electrode and from the connecting cables to the cathode-follower are investigated.

As in general the beam influences charges all over the electrode, a continous distribution of current generators may be assumed. Here, in approximation, 5 equivalent circuit generators are assumed at points B, C, D, E, and F, with the respective currents i_{KB}, i_{KC}, i_{KD}, i_{KE}, and i_{KF} (see Fig. 37).

The load-independent current is

$$i_{K\nu} = \frac{dq_\nu}{dt} \qquad (\nu = B, C, D, E, F)$$

or, in case of a sine-wave current

$$i_{K\nu} = q_\nu j\omega \quad .$$

The characteristic impedance on the electrode is not constant. According to ref. [9] the curve shown in Fig. 37 results from the geometrical data

$$Z_L = \frac{377}{\sqrt{\epsilon_r}} \cdot \frac{d}{b+d} \qquad (70)$$

d = thickness, b = width } of the electrode

ϵ_r = dielectric constant

The 75 ohm supply cable is terminated by the input impedance of the cathode-follower $R_g \,||\, C$ in series with an unavoidable inductivity L and a loss resistance R_2. Via the supply cable this terminating impedance is transformed dependent on frequency. This dependence is shown in the Smith diagrams

Figs. 38-41 for points A, B, C, D, E, and F, (see Fig. 37), with R_g = 2 MΩ, C = 10 pF, L = 30 nH and R_2 = 75 ohms). Within the electrode the line transformation was done with mean characteristic impedances.

The current i_2 in the output impedance Z_2 (see Fig. 42) is caused by a superposition of all currents coming from the 5 current generators :

$$i_2 = \sum_{\nu=B}^{F} i_{2\nu} \qquad (\nu = B, C, D, E, F) \qquad (71)$$

Assuming that $f >> \frac{1}{2\pi R_g C}$, the output voltage becomes

$$U_3 = i_2 \cdot \frac{1}{j\omega C} \qquad (72)$$

For the frequencies ($f << \frac{1}{2\pi R_g C}$) :

$$U_{3\ell} = \frac{q_{tot}}{C_{tot}} \qquad (73)$$

with

$$C_{tot} = C_{electrode} + C_{cable} + C$$

and

$$q_{tot} = \Sigma q_\nu$$

Consequently, the resonance distortion becomes

$$\frac{U_3}{U_{3\ell}} = \frac{i_2 \cdot C_{tot}}{j\omega C \, q_{tot}} = \frac{\Sigma i_{2\nu}}{\Sigma i_{K\nu}} \cdot \frac{C_{tot}}{C} \qquad (74)$$

Current $i_{2\nu}$ can be determined by means of the impedance curves Figs. 38-41 and by the principle of continuous real power.

$$i_{1\nu}^{\,2} R_{1\nu} = i_{2\nu}^{\,2} R_2$$

$$i_{2\nu} = i_{1\nu} \sqrt{\frac{R_{1\nu}}{R_2}} \qquad \text{(see Fi. 42)} \qquad (75)$$

Allowing for the open electrode end which has the effect of a shunt reactance X_p (see Fig. 42), it follows that

$$i_{1\nu} = i_{K\nu} \cdot \frac{jX_{p\nu}}{R_{1\nu} + j(X_{1\nu} + X_{p\nu})}$$

and thus

$$i_{2\nu} = i_{K\nu} \cdot \sqrt{\frac{R_{1\nu}}{R_2}} \frac{jX_{p\nu}}{R_{1\nu} + j(X_{1\nu} + X_{p\nu})}$$

The currents $|i_{2\nu}|$ coming from the generator points ν (ν = B, C, D, E, and F) are plotted in Fig. 43 as a function of frequency.

Due to the difference in electrode lengths in point B, C, D, E, and F the influenced charges, or generator currents respectively, in these points are also different.

On the average the ratio between these currents equals the ratio between the electrode lengths :

$$i_{kB} : i_{kC} : i_{kD} : i_{KE} : i_{kF} = 0,7 : 3 : 4 : 3 : 0,7$$

Bearing this in mind, the total output voltage excess $\frac{U_3}{U_{3l}}$ as assessed in equation (74) is as plotted in Fig. 44. Thus, the maximal signal excess up to f = 600 MHz is less than 3, which corresponds to 10 db.

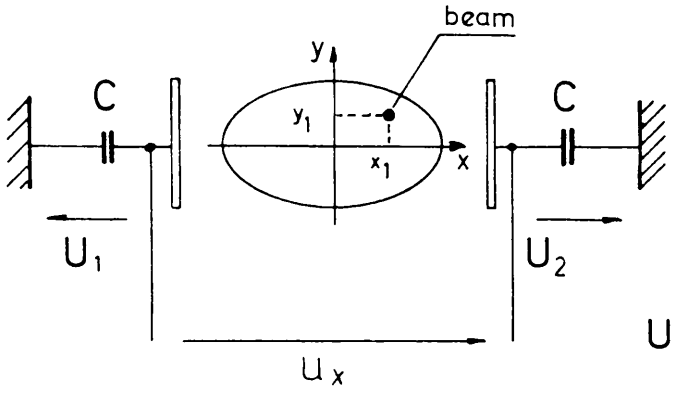

Fig. 1

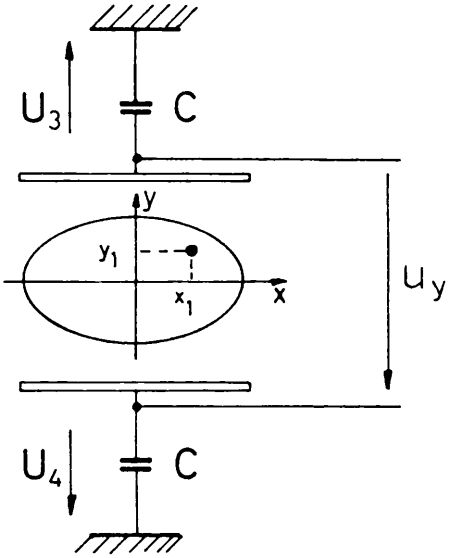

Fig. 2

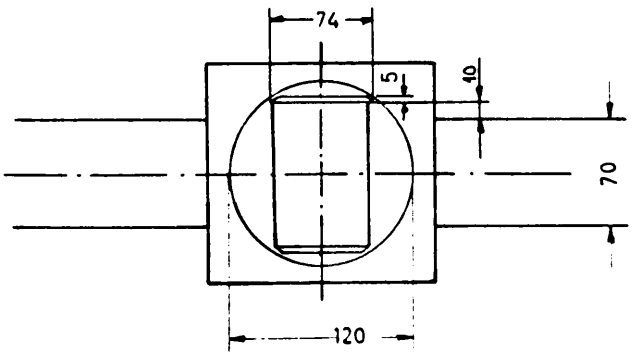

Fig. 3

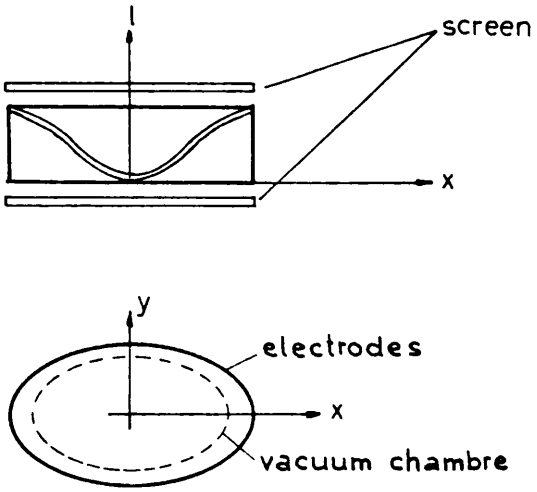

Fig. 4

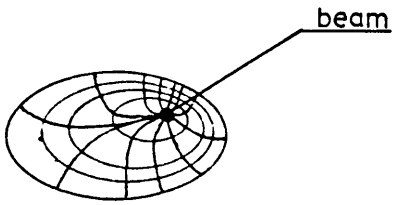

Fig. 5

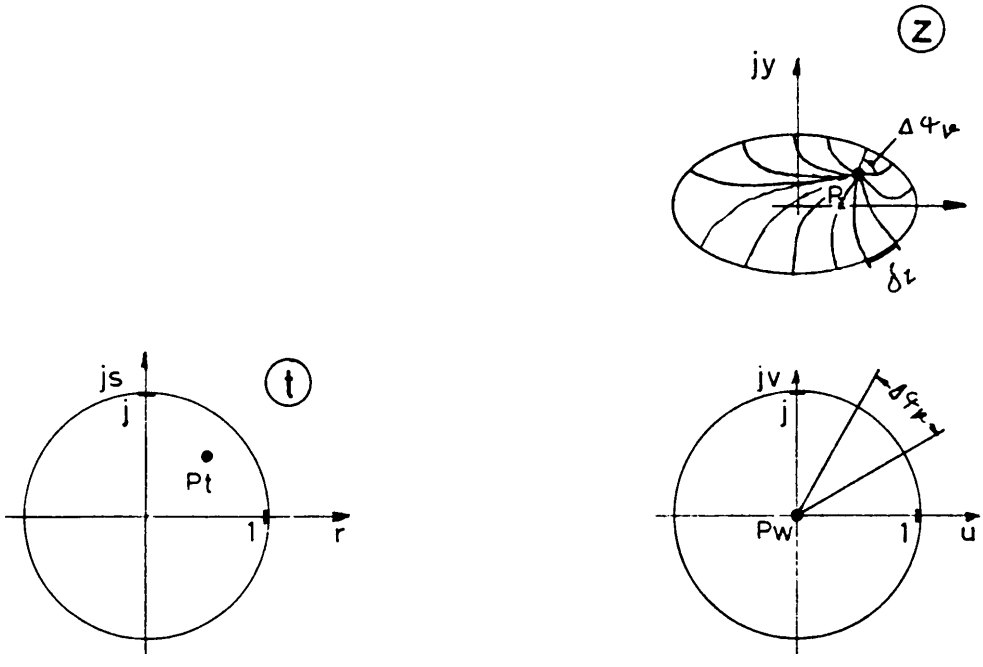

Fig. 6

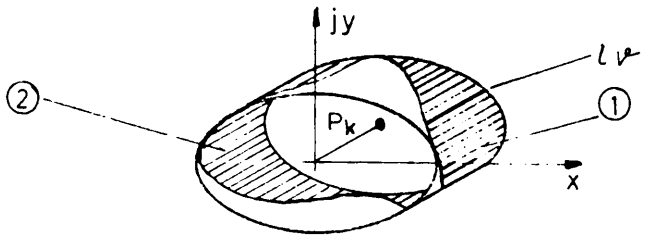

Fig. 7

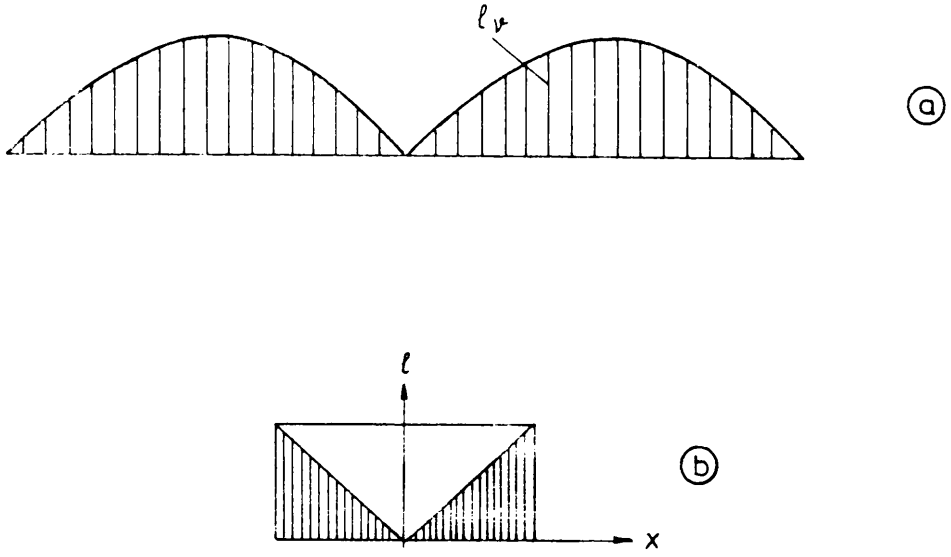

Fig. 8

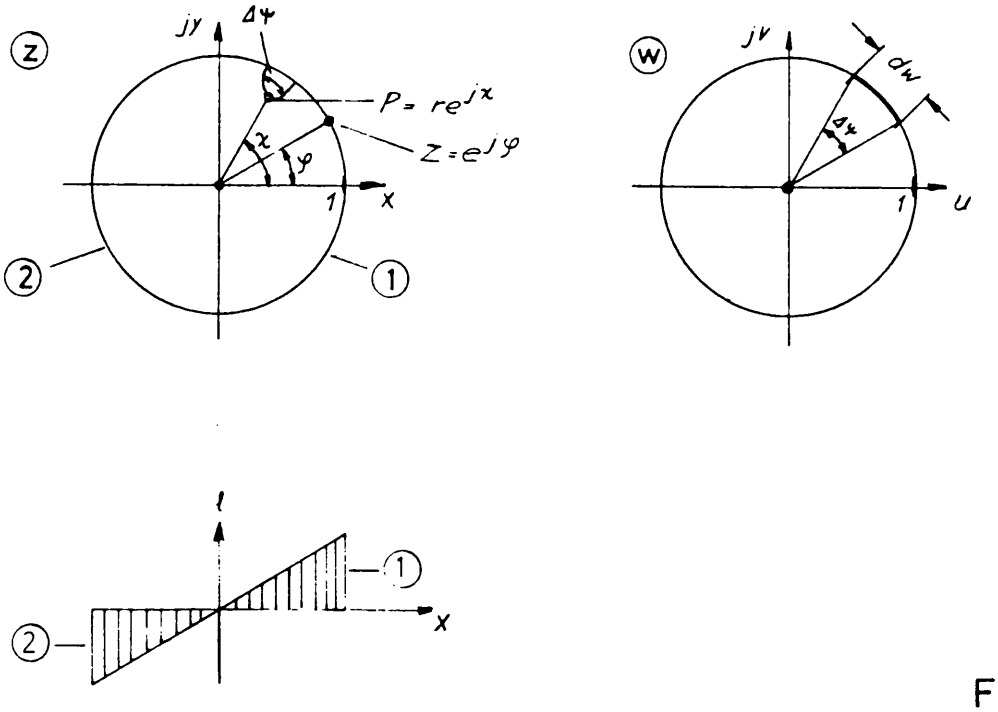

Fig. 9

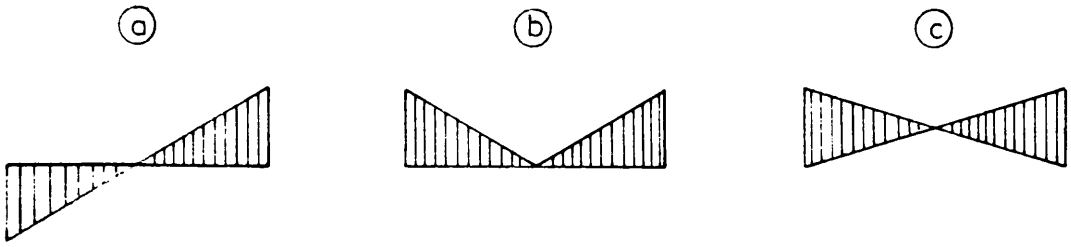

Fig. 10

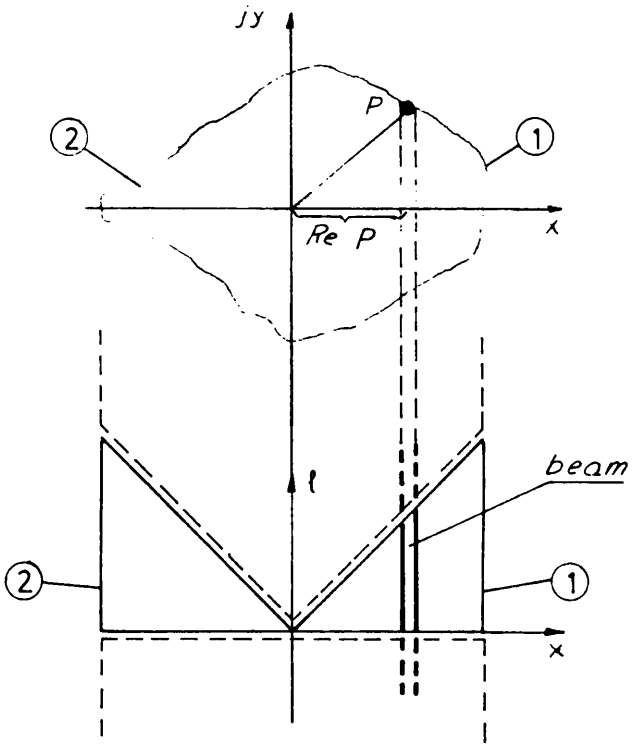

Fig. 11

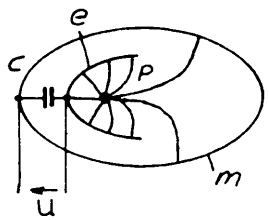

e = electrode

p = beam position

m = mass

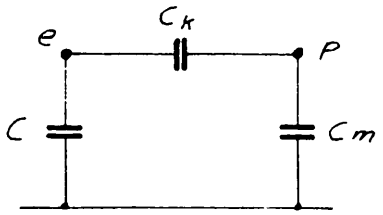

ⓐ ⓑ

Fig. 12

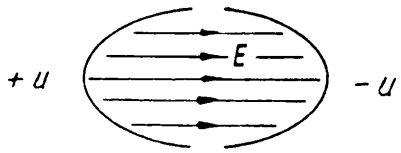

Fig. 13

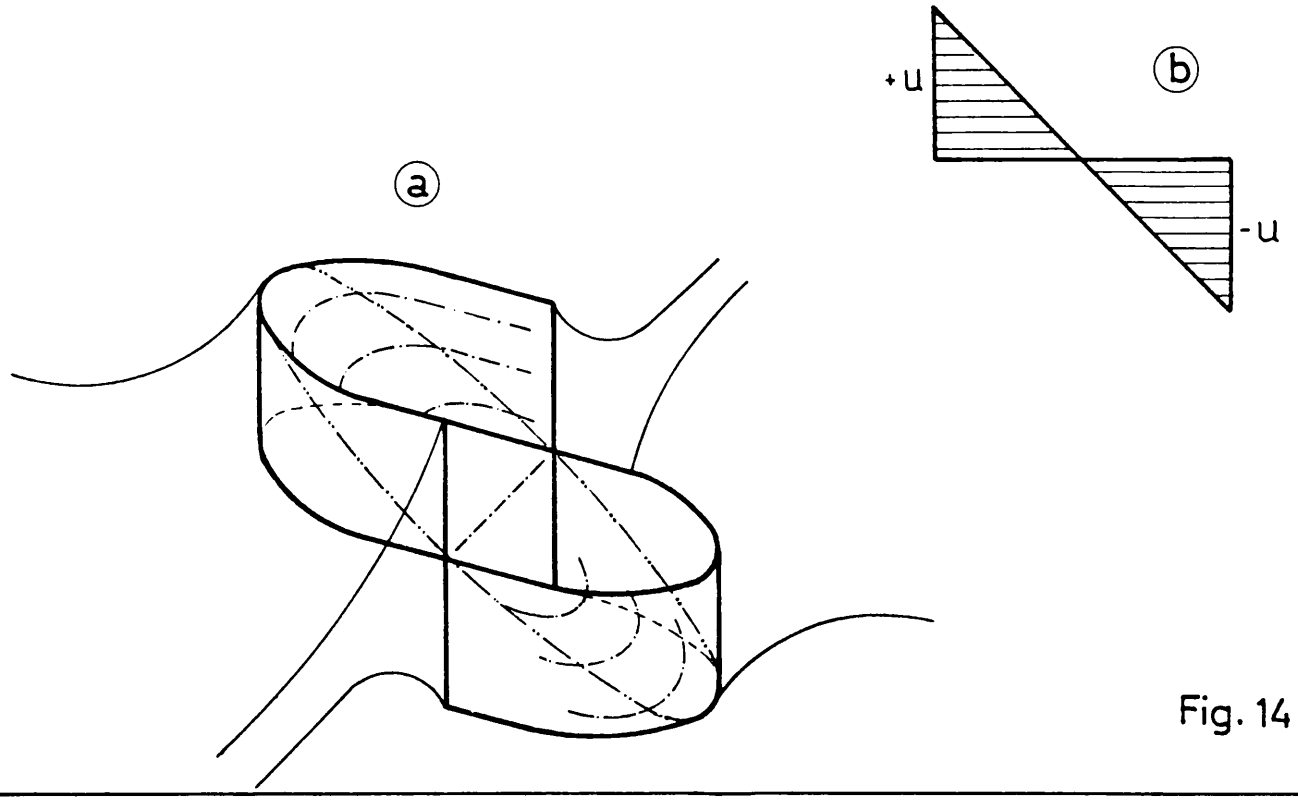

Fig. 14

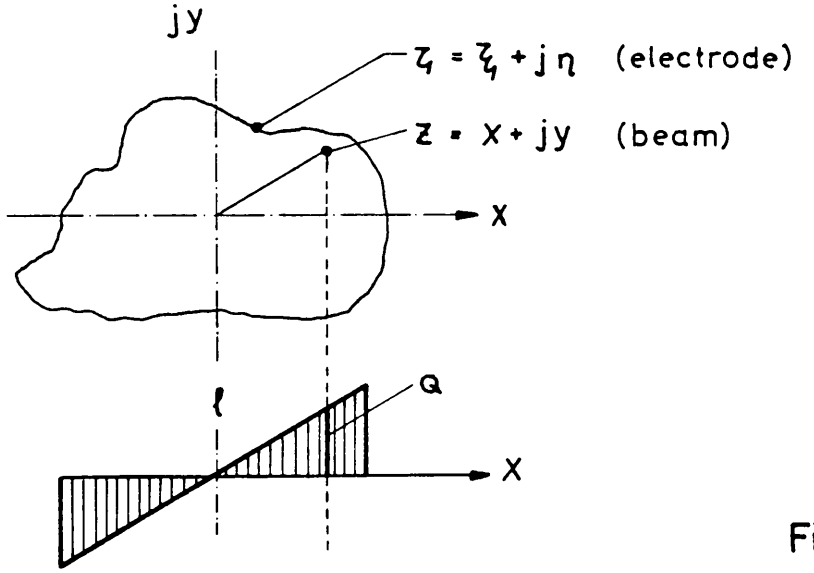

Fig. 15

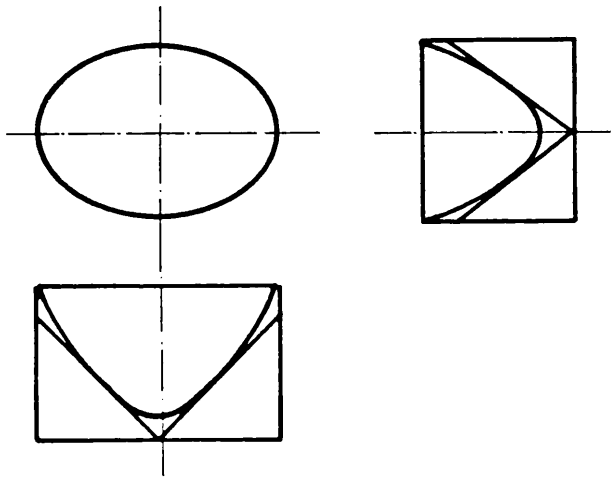

Fig. 16

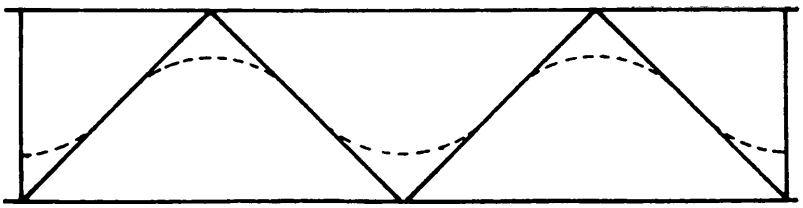

a

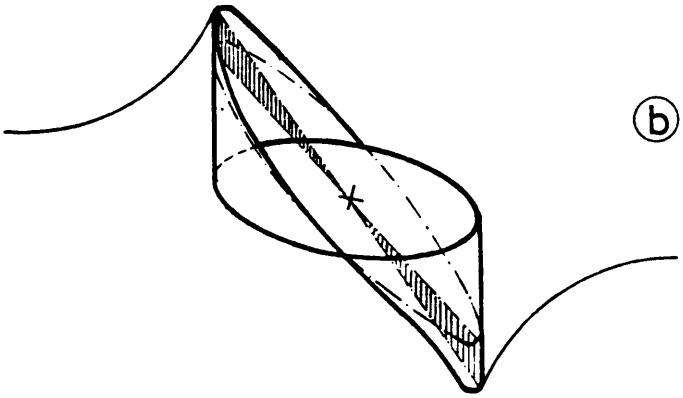

b

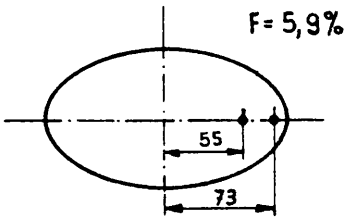

c

Fig. 17

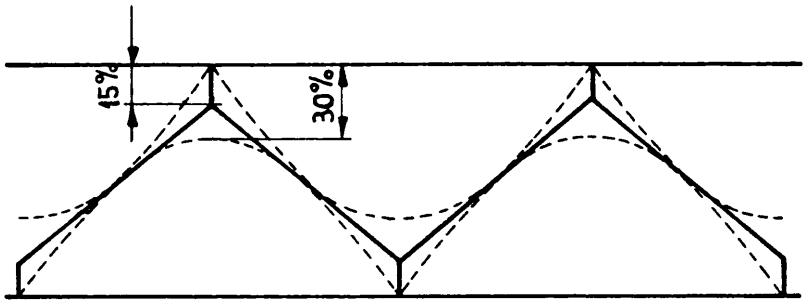

a

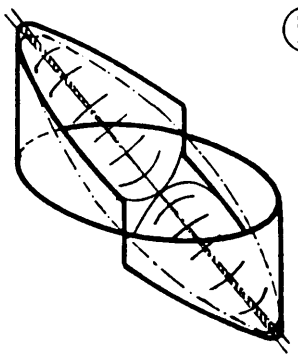

b

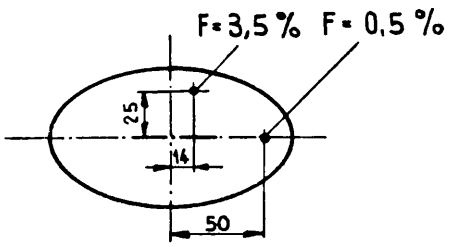

c

Fig. 18

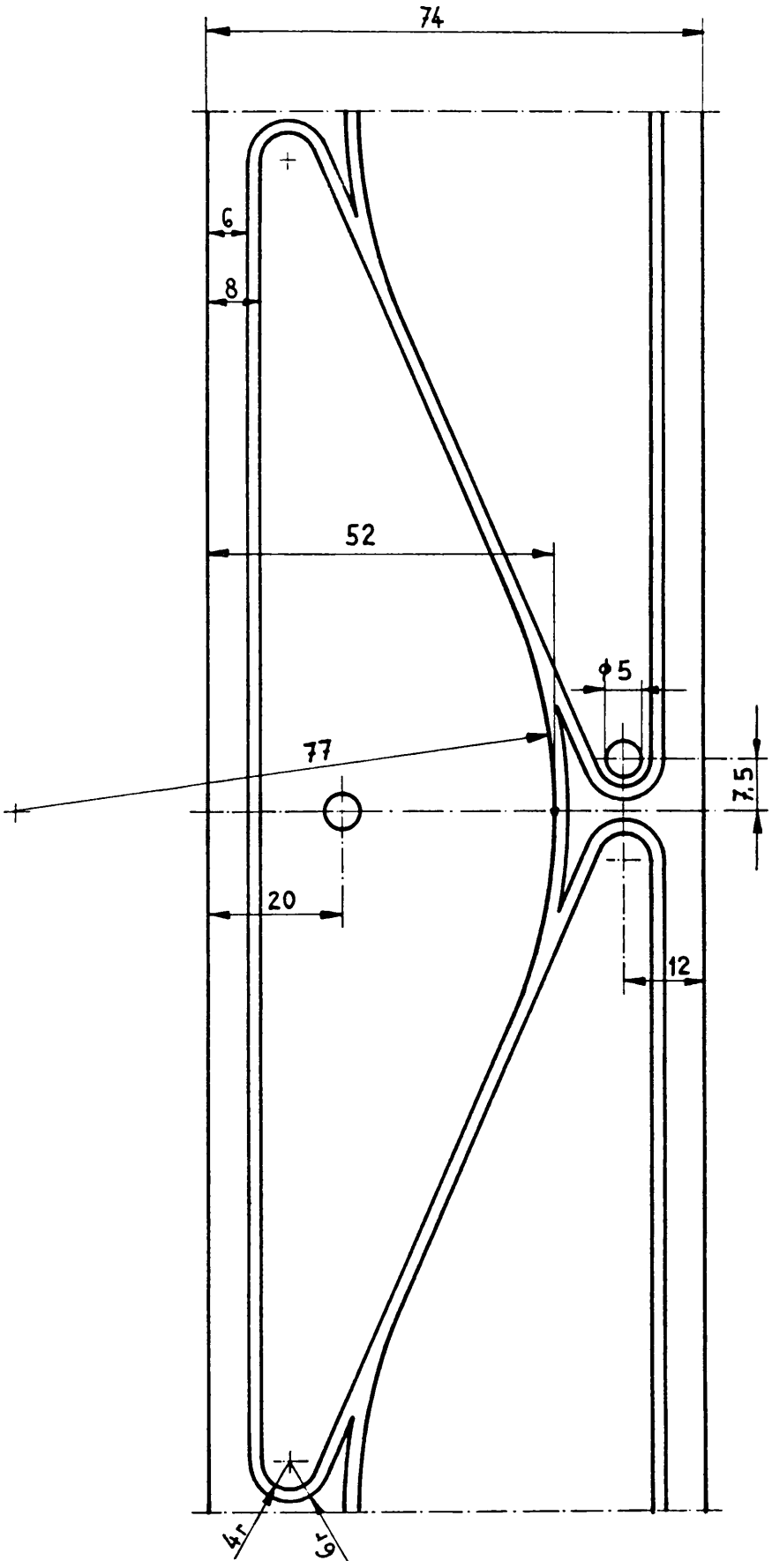

Fig. 19

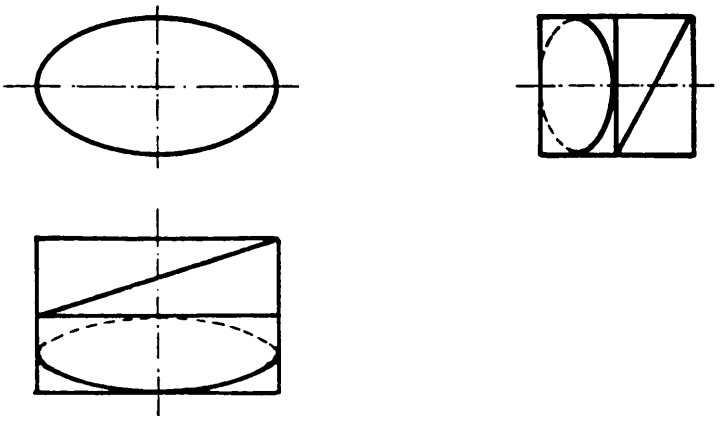

Fig. 20

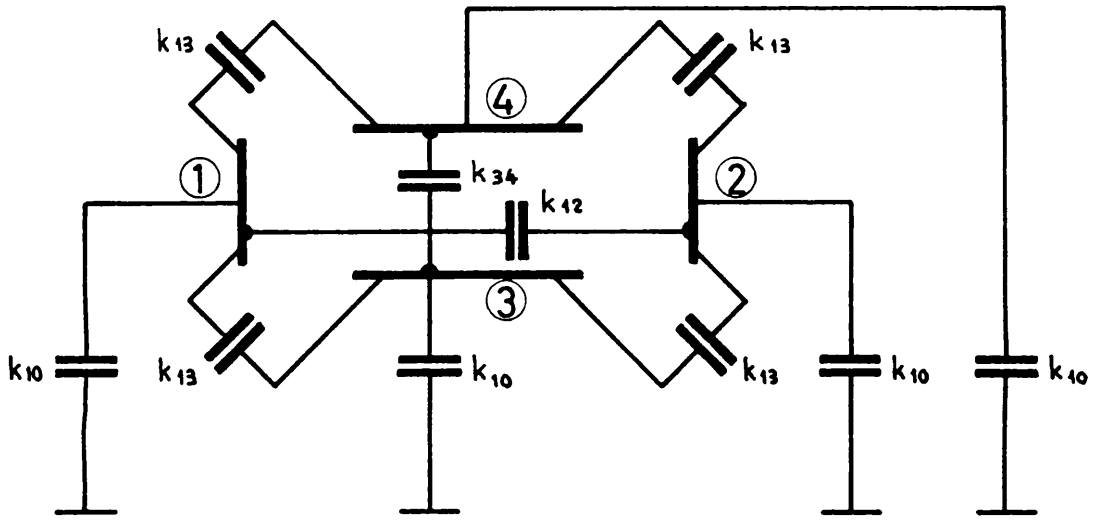

Fig. 21

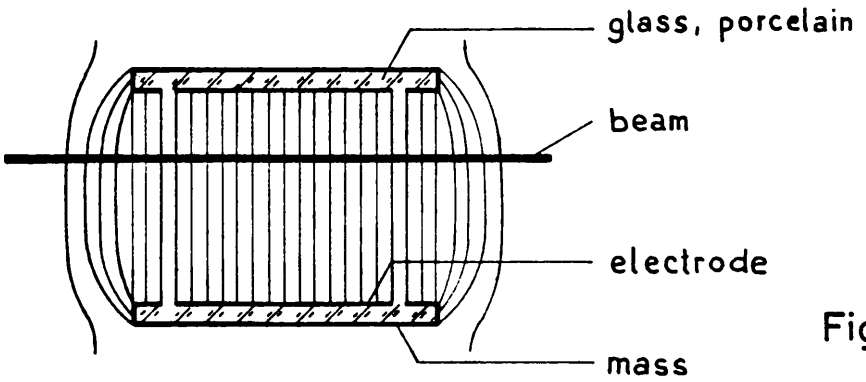

Fig. 22

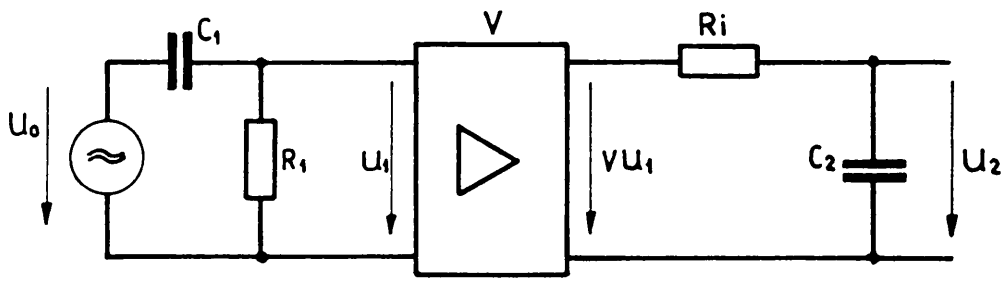

Fig. 23

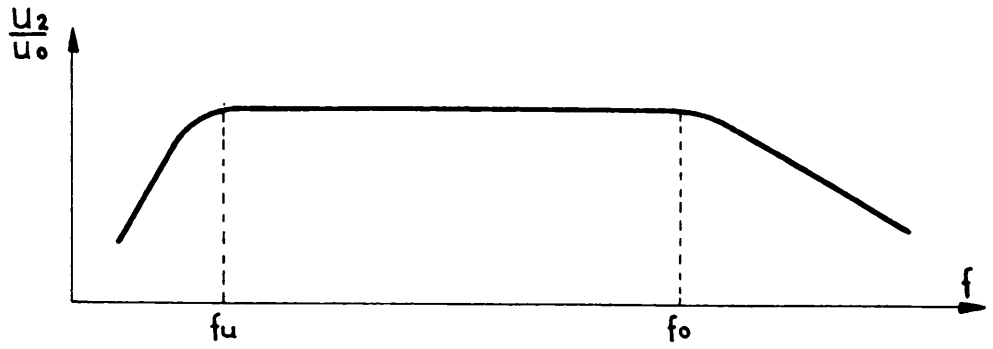

Fig. 24

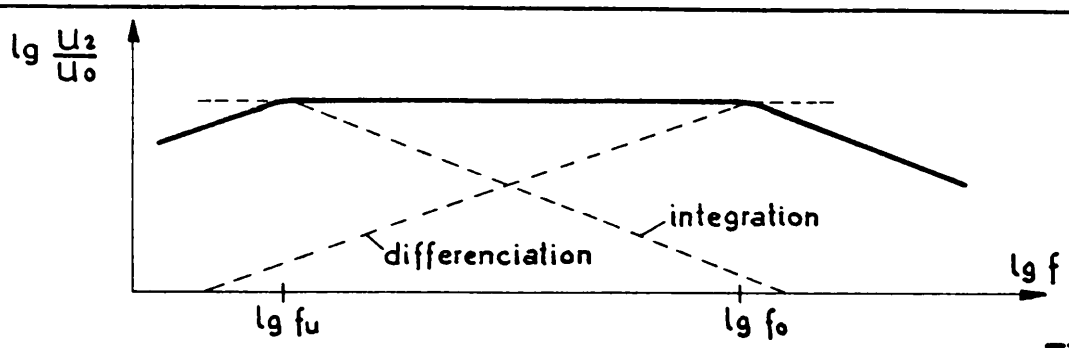

Fig. 25

$$Ri = \frac{Ri_{Rö} \cdot Ra}{Ri_{Rö} + Ra}$$

S	=	50 mA/V
Ra	=	100 kΩ
$Ri_{Rö}$	=	100 kΩ
C_2	=	300 pF
R_1	=	75 Ω
C_1	=	100 pF
Rö	=	E810F

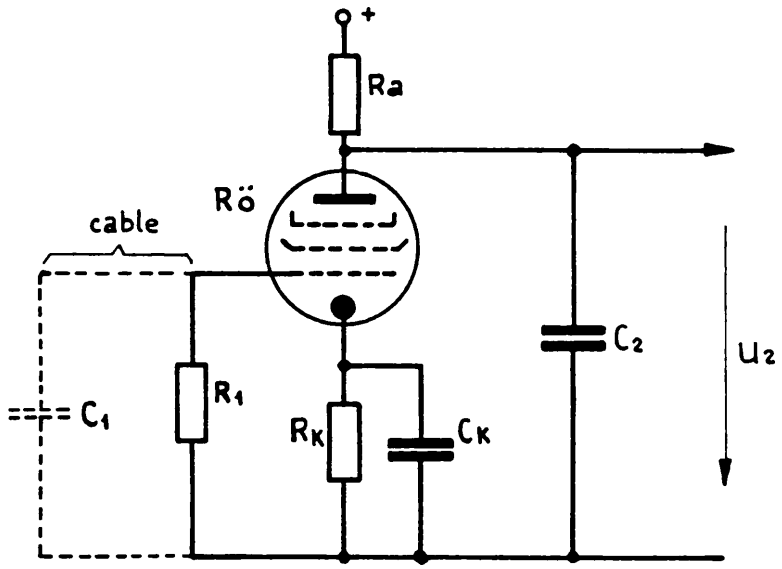

Fig. 26

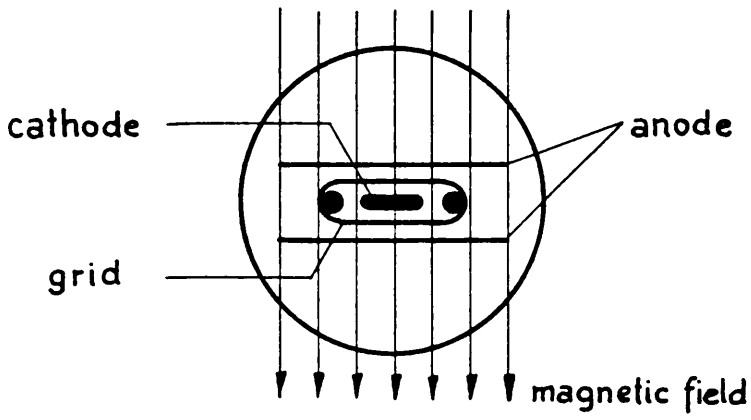

Fig. 27

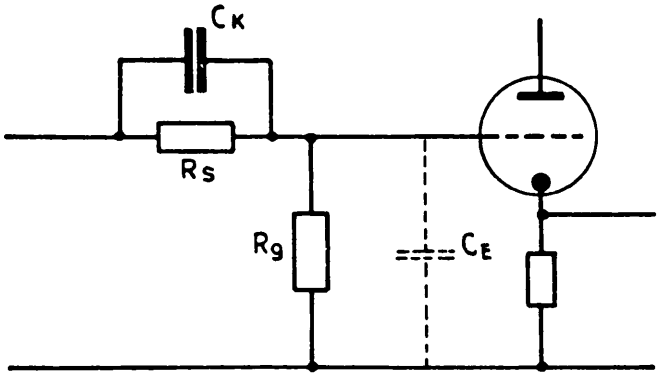

Fig. 28

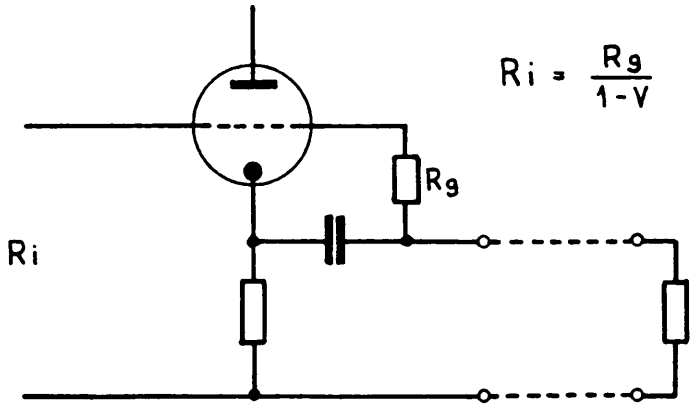

Fig. 29

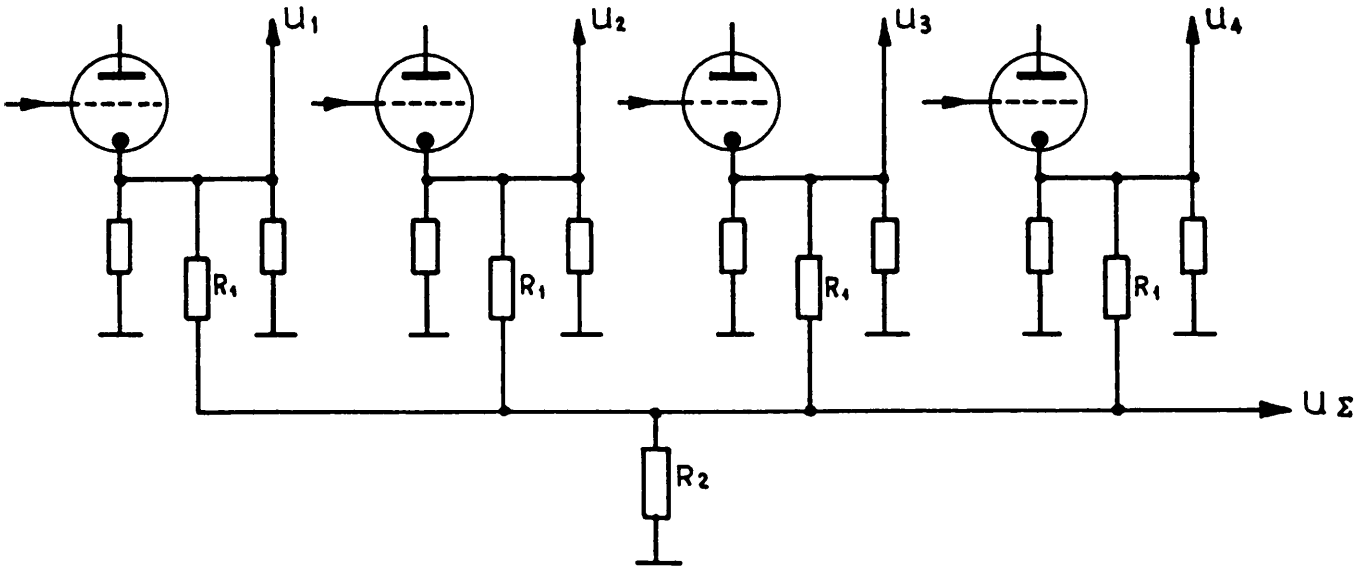

Fig. 30

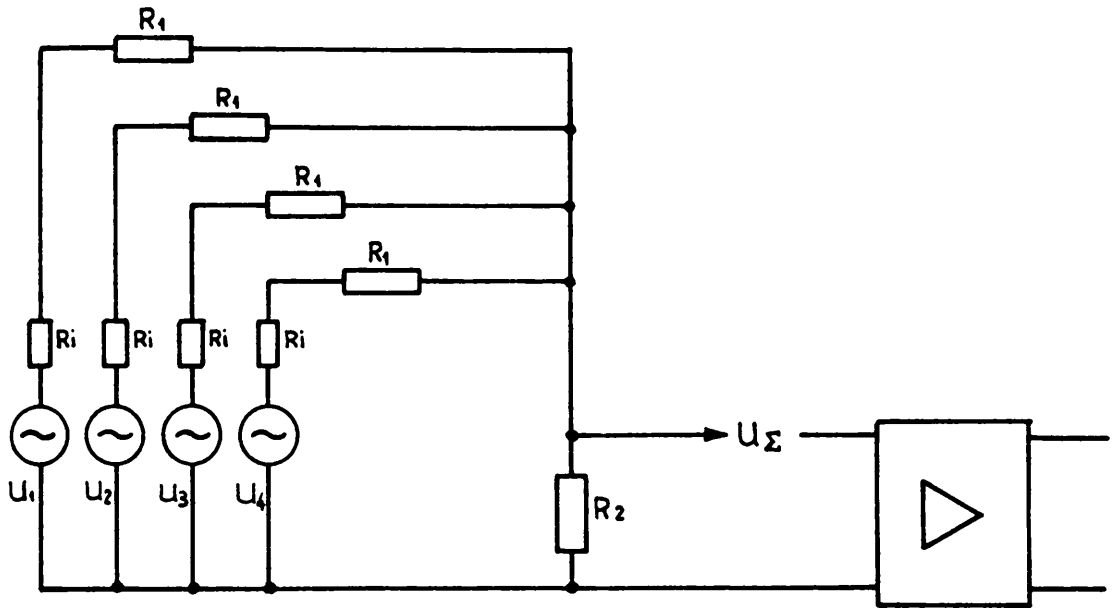

Fig. 31

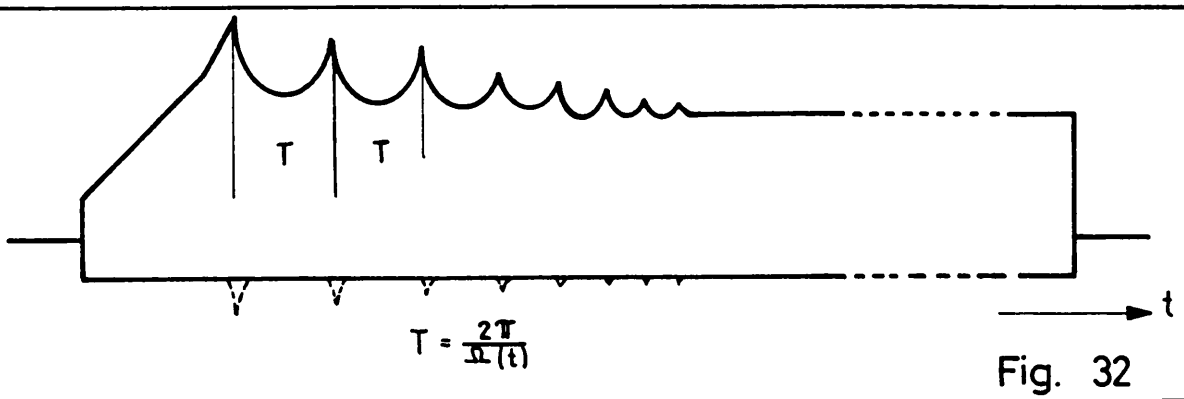

Fig. 32

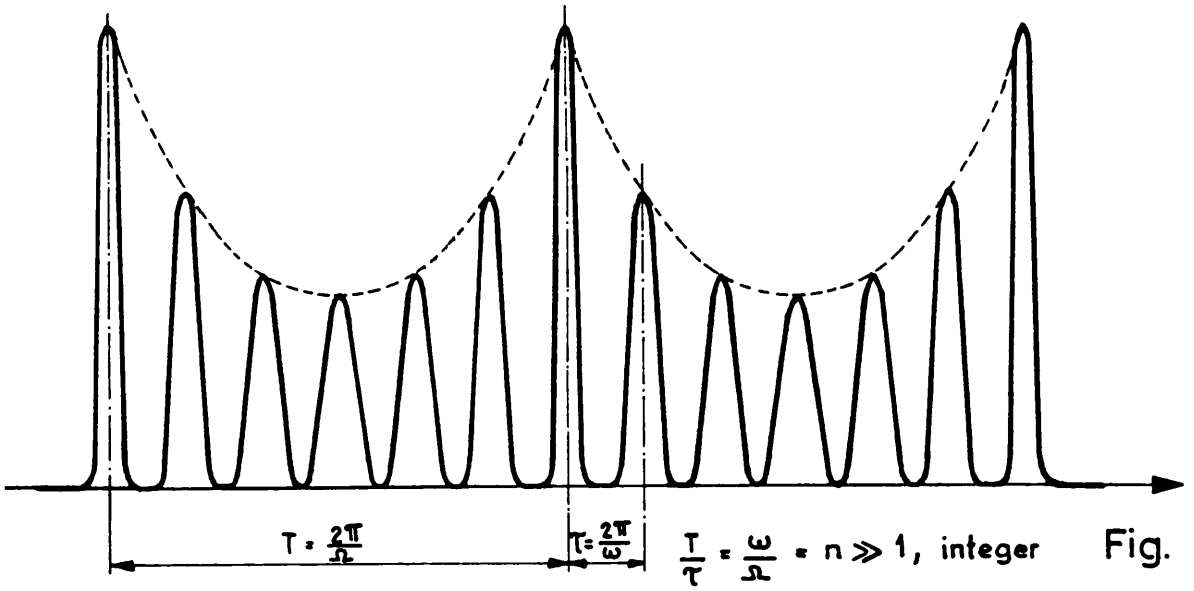

Fig. 33

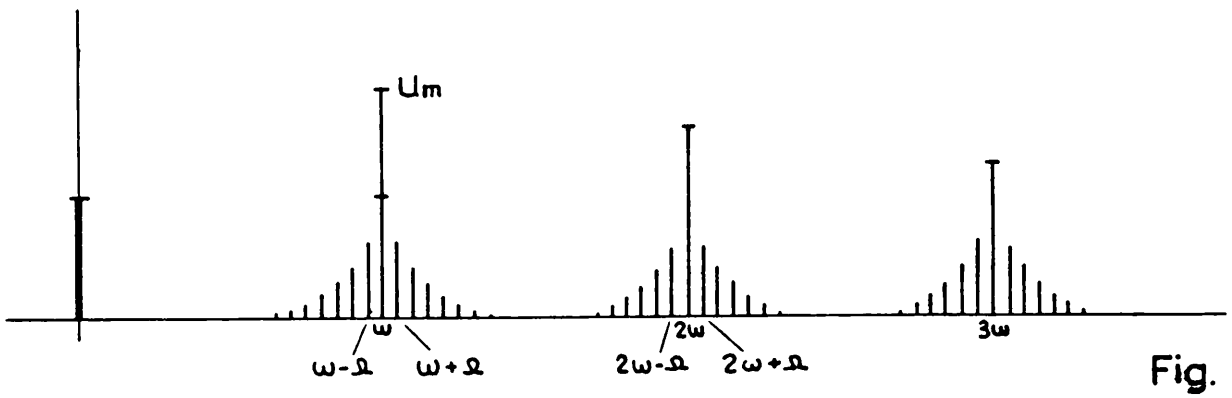

Fig. 34

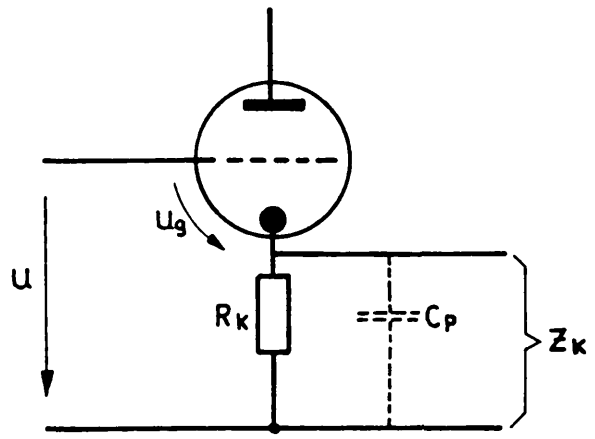

Fig. 35

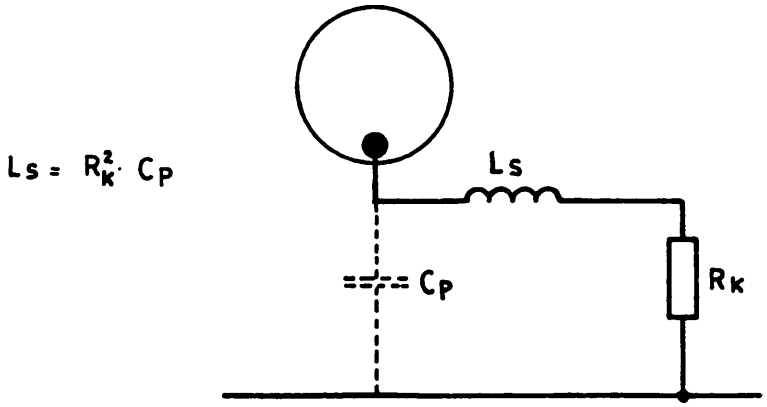

Fig. 36

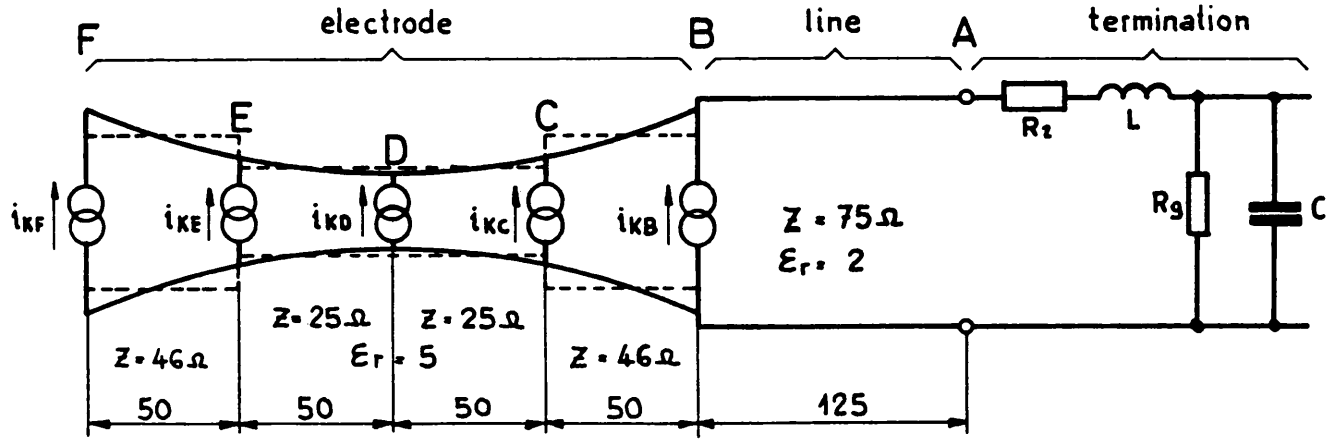

Fig. 37

NAME	TITLE	DWG. NO.
		DATE
SMITH CHART FORM #28SPR (2-49)	KAY ELECTRIC COMPANY, PINE BROOK, N.J. ©1949 PRINTED IN U.S.A.	

IMPEDANCE OR ADMITTANCE COORDINATES

$Z_L = 75\,\Omega$

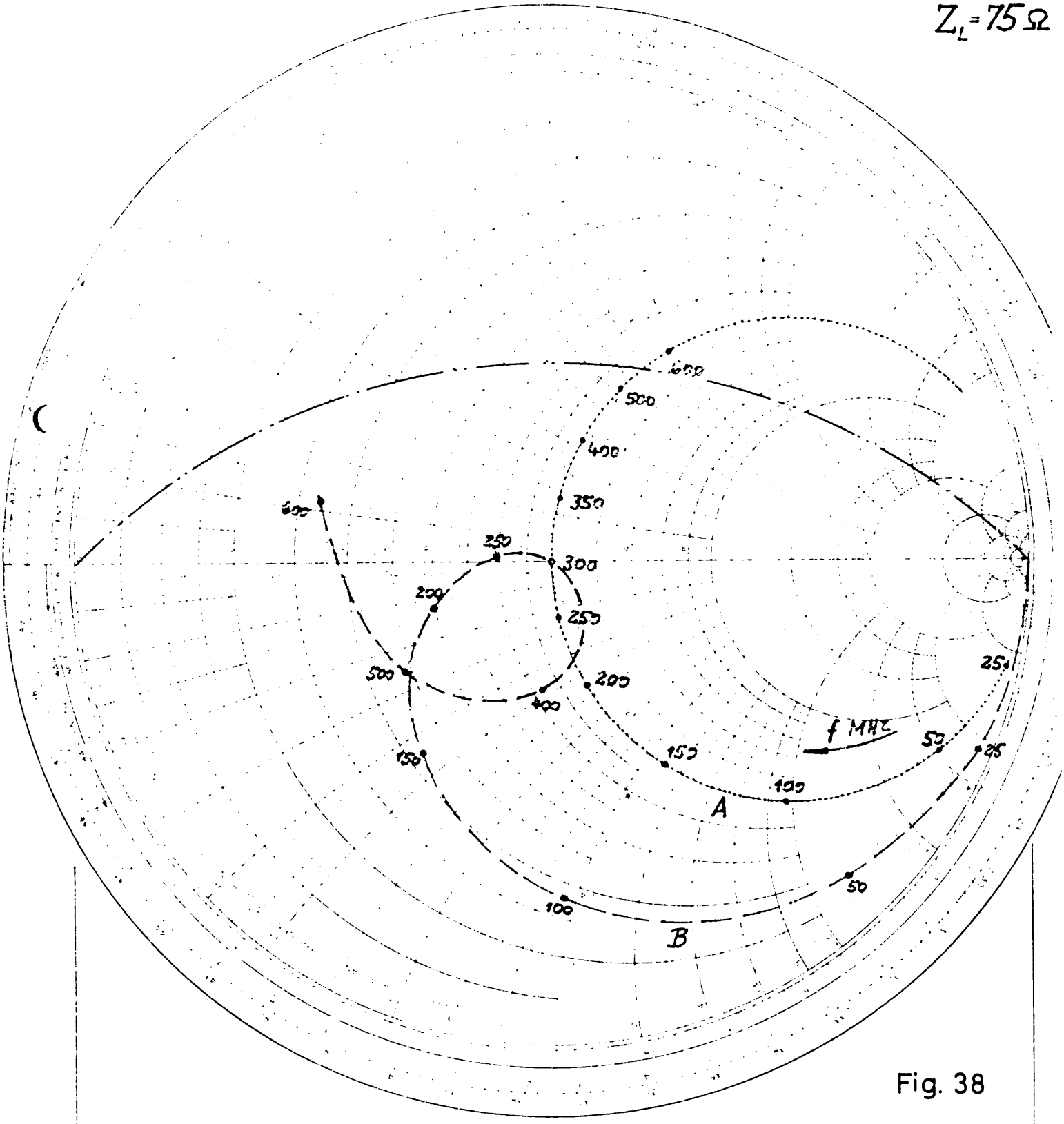

Fig. 38

RADIALLY SCALED PARAMETERS

TOWARD GENERATOR

TOWARD LOAD

CENTER

STANDING WAVE RATIO

TRANSM. LOSS

ELECTRONICS - VOL. 17, NO. 1, PP. 130-133, 318-325, JAN. 1944

NAME	TITLE	DWG. NO.
SMITH CHART FORM 82BSPR (2-49)	KAY ELECTRIC COMPANY, PINE BROOK, N.J. ©1949 PRINTED IN U.S.A.	DATE

IMPEDANCE OR ADMITTANCE COORDINATES

$Z_{BC} = 46\,\Omega$

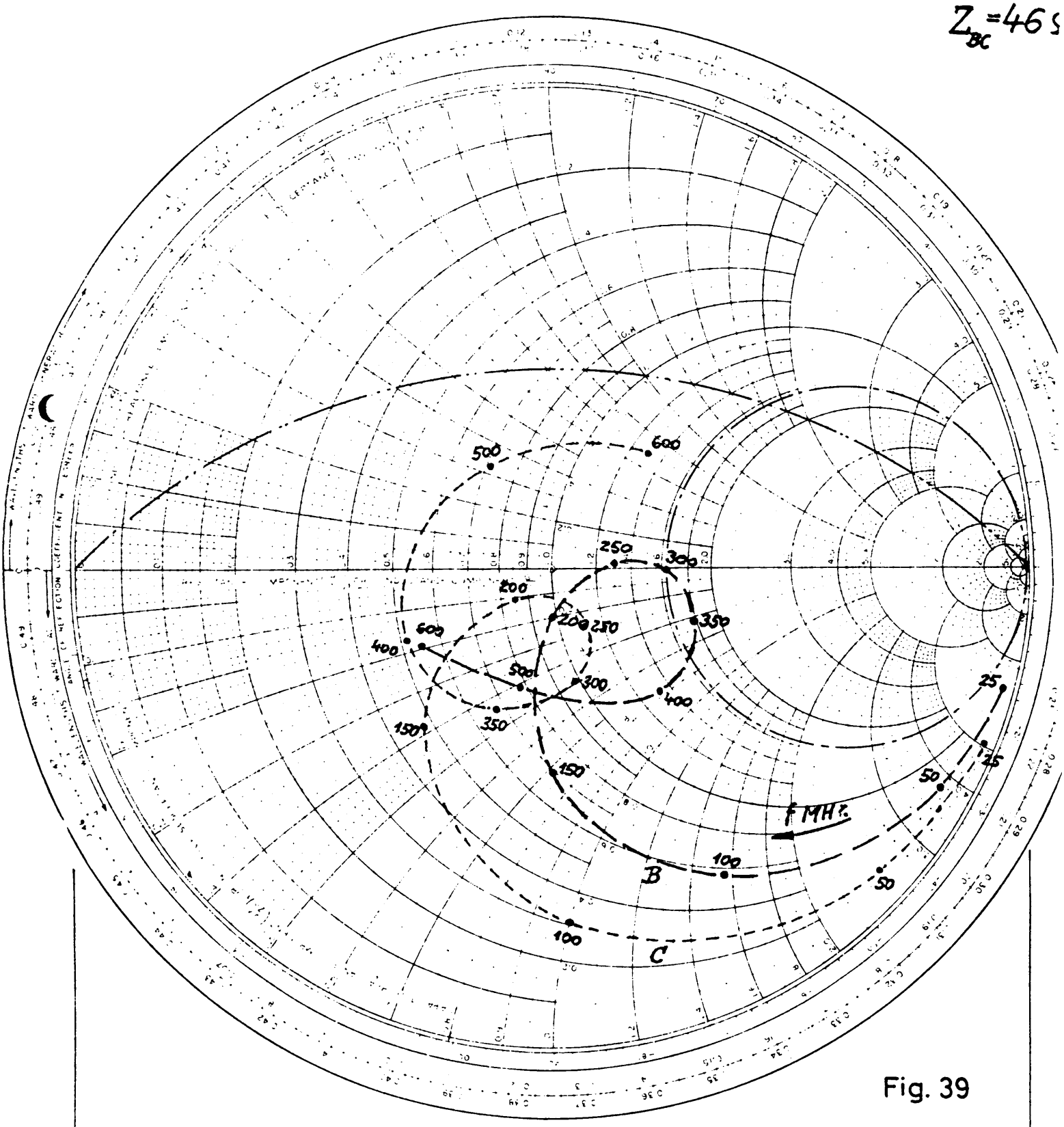

Fig. 39

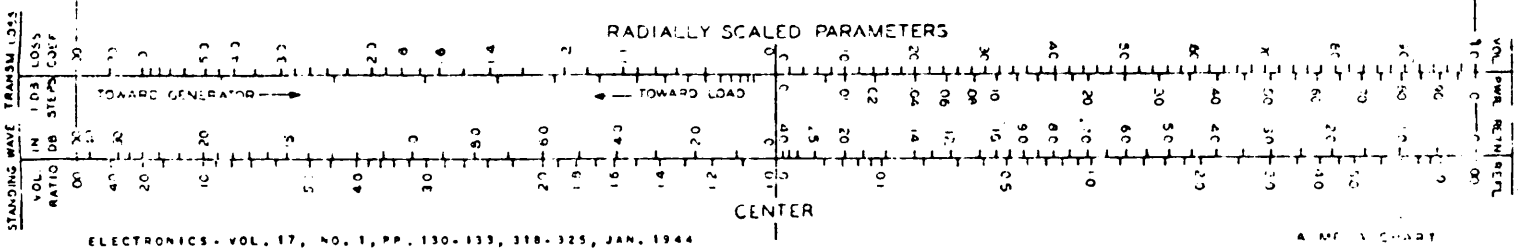

ELECTRONICS - VOL. 17, NO. 1, PP. 130-133, 318-325, JAN. 1944

SIS/R/10920

NAME	TITLE	DWG. NO.
		DATE
SMITH CHART FORM 828SPR (2-49)	KAY ELECTRIC COMPANY, PINE BROOK, N.J. © 949 PRINTED IN U.S.A.	

IMPEDANCE OR ADMITTANCE COORDINATES

$Z_{CD} = Z_{DE} = 25$

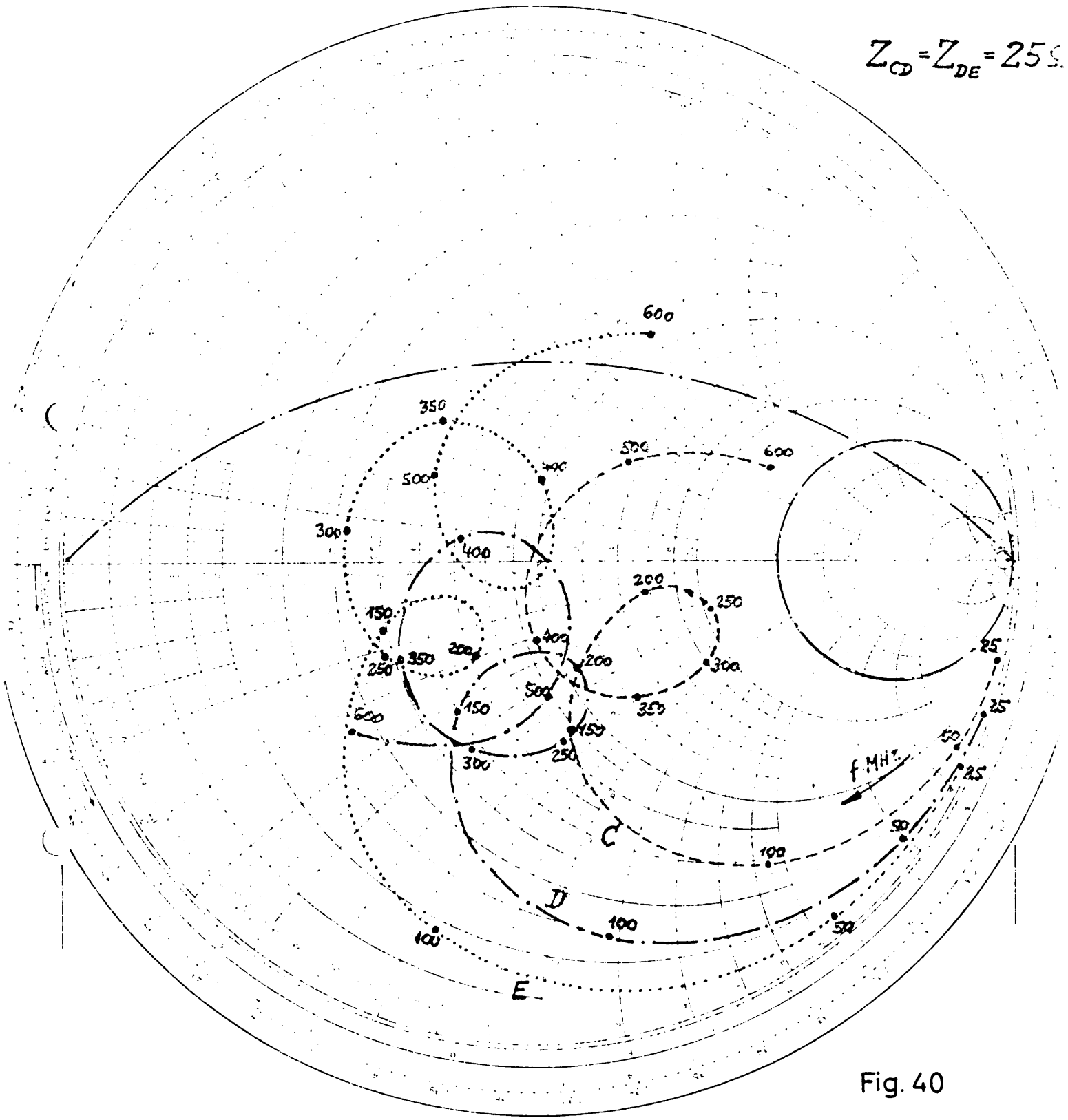

Fig. 40

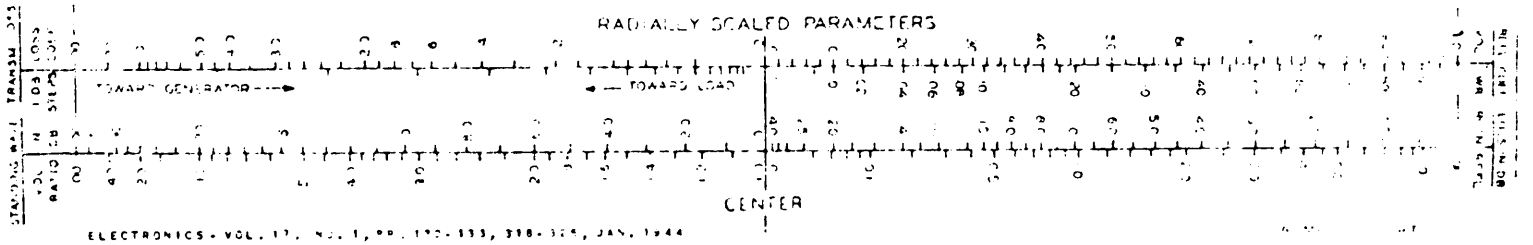

ELECTRONICS - VOL. 17, NO. 1, PP. 130-133, 318-324, JAN. 1944

SIS/R/10923

NAME	TITLE	DWG. NO.
		DATE
SMITH CHART FORM 828SPR (2-49)	KAY ELECTRIC COMPANY, PINE BROOK, N.J. ©1949 PRINTED IN U.S.A.	

IMPEDANCE OR ADMITTANCE COORDINATES

$Z_{EF} = 46\ \Omega$

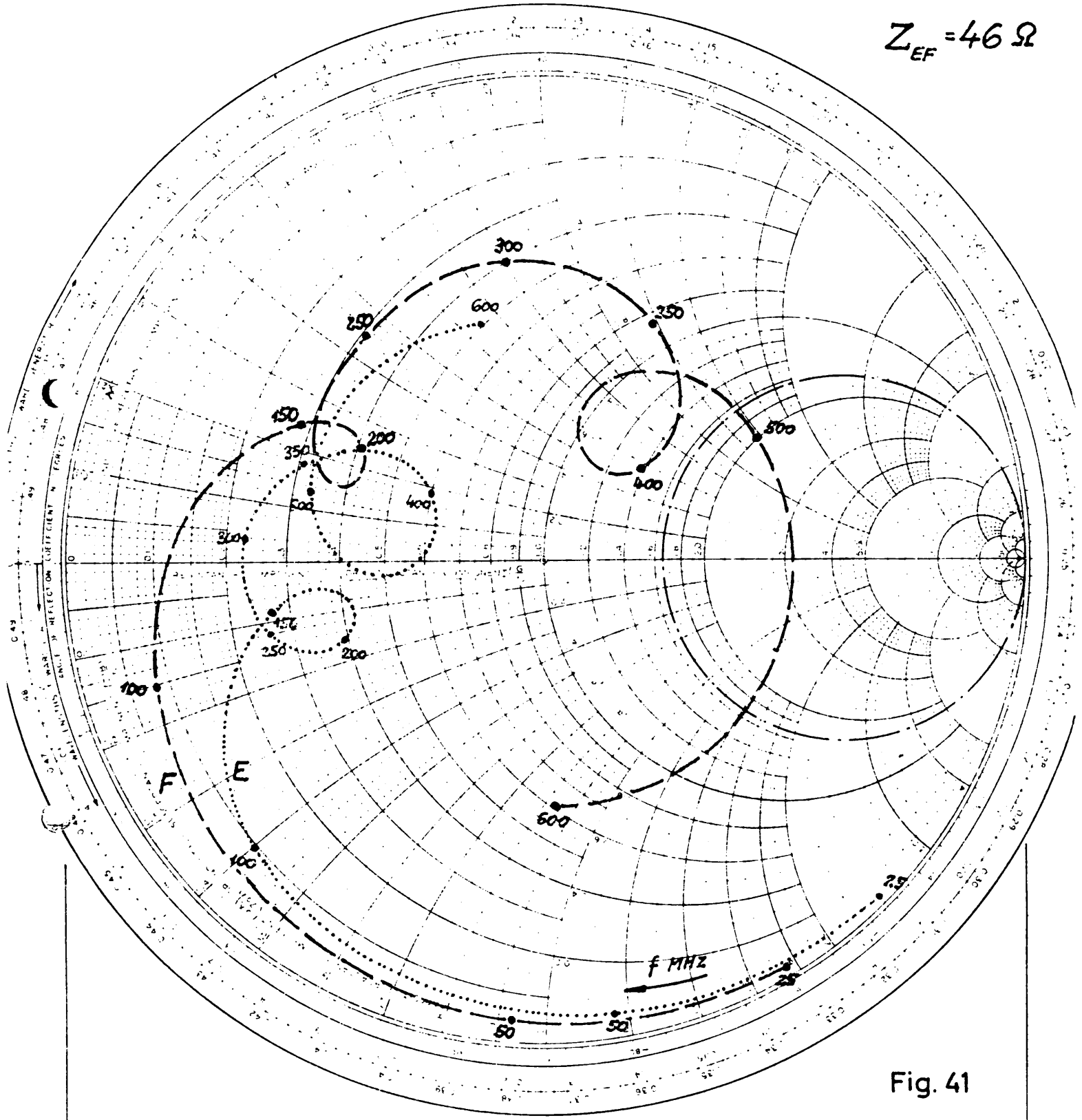

Fig. 41

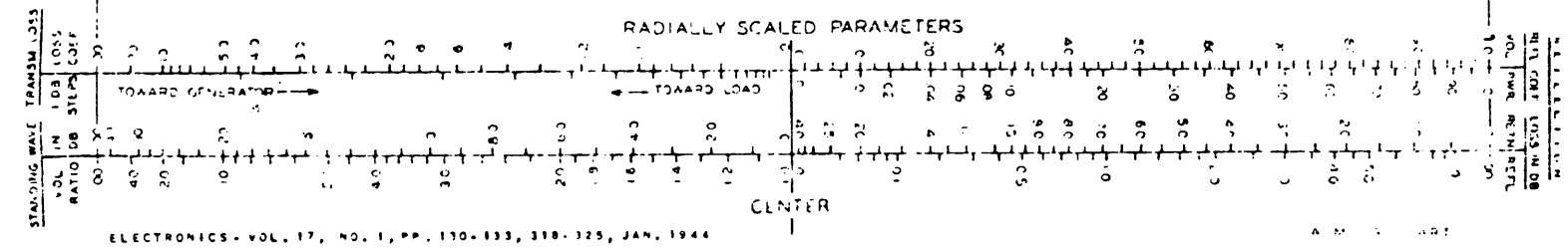

ELECTRONICS - VOL. 17, NO. 1, PP. 130-133, 318-325, JAN. 1944

SIS/R/10921

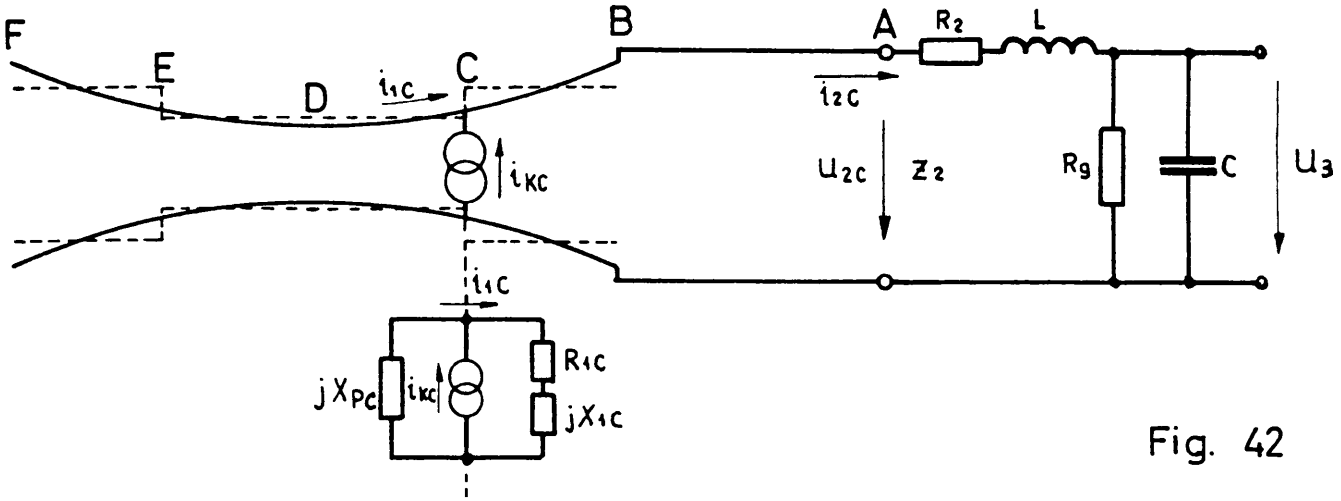
F
E
D
C
B
A
R_2
L
i_{1C}
i_{KC}
i_{2C}
U_{2C}
Z_2
R_g
C
U_3
jX_{PC}
R_{1C}
jX_{1C}

Fig. 42

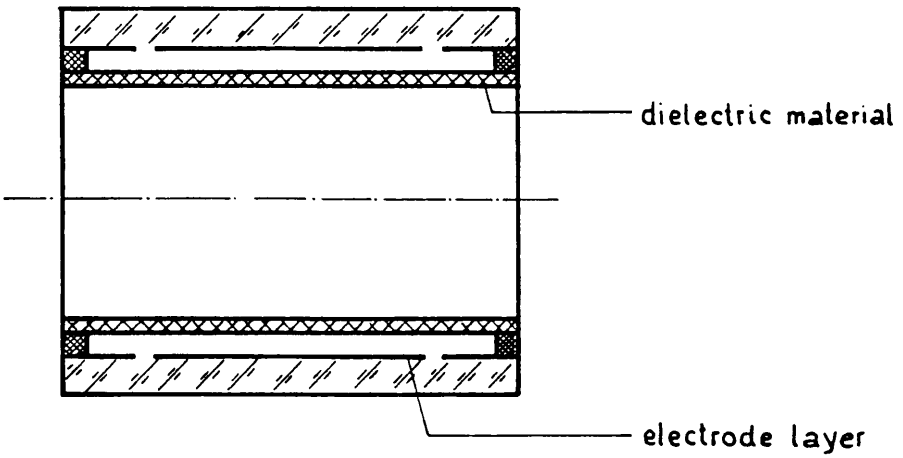
dielectric material
electrode layer

Fig. 45

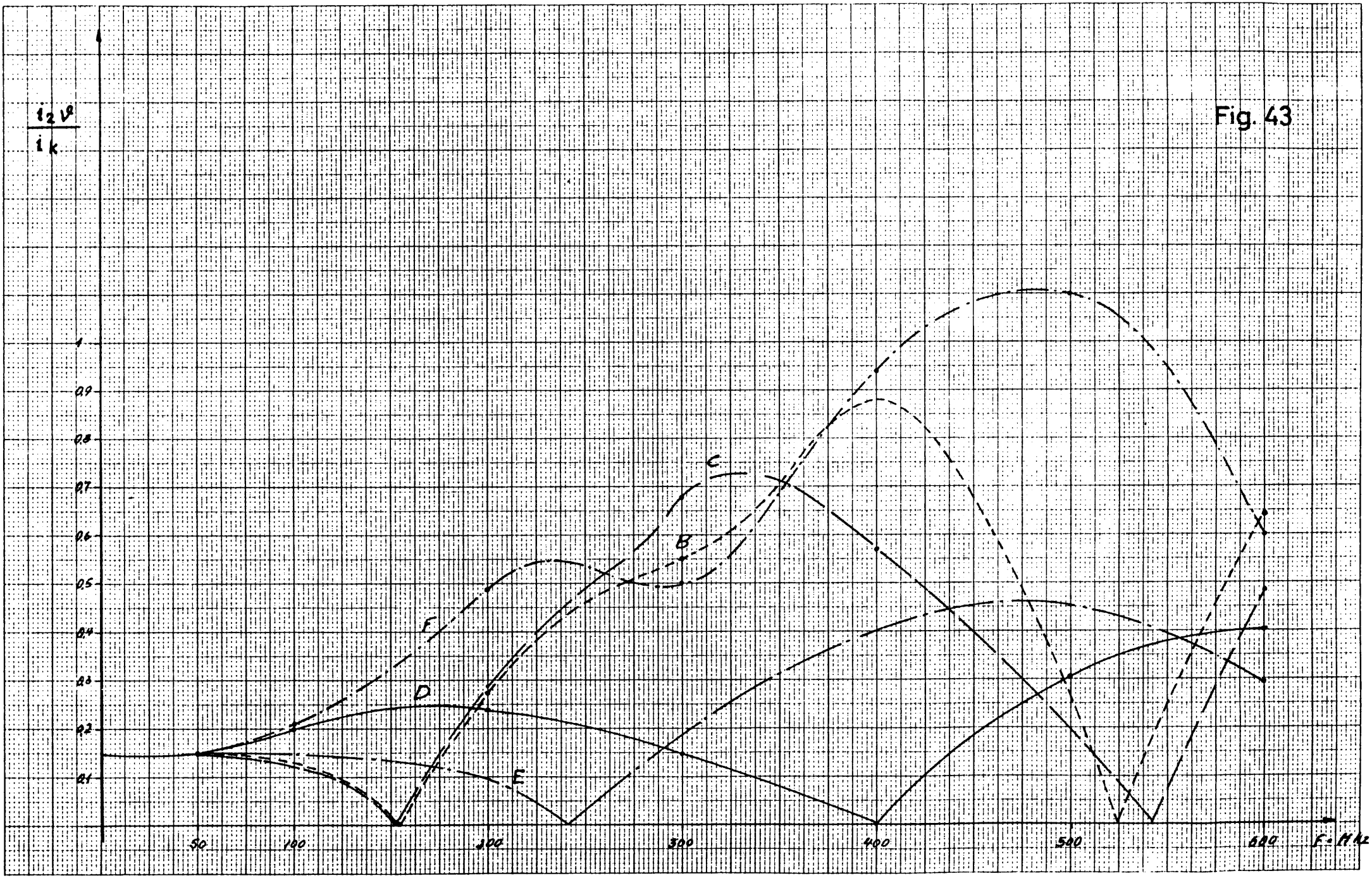
Fig. 43
$\frac{i_2 v^2}{i_k}$
1
0,9
0,8
0,7
0,6
0,5
0,4
0,3
0,2
0,1
50
100
200
300
400
500
600
F - MHz
A
B
C
D
E
F

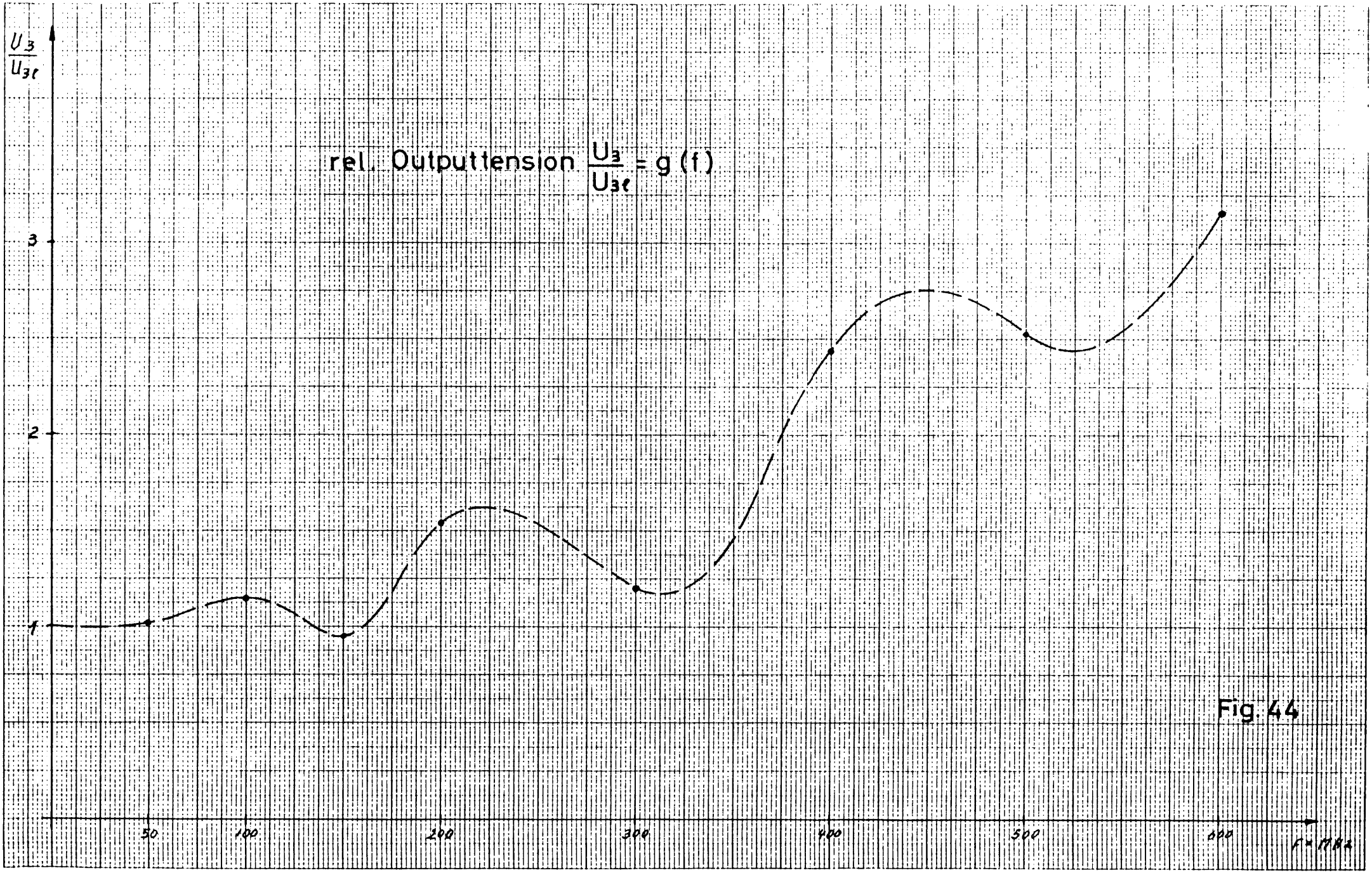
rel. Outputtension $\frac{U_3}{U_{3\ell}} = g(f)$
$\frac{U_3}{U_{3\ell}}$
3
2
1
50
100
200
300
400
500
600
f = MHz

Fig. 44

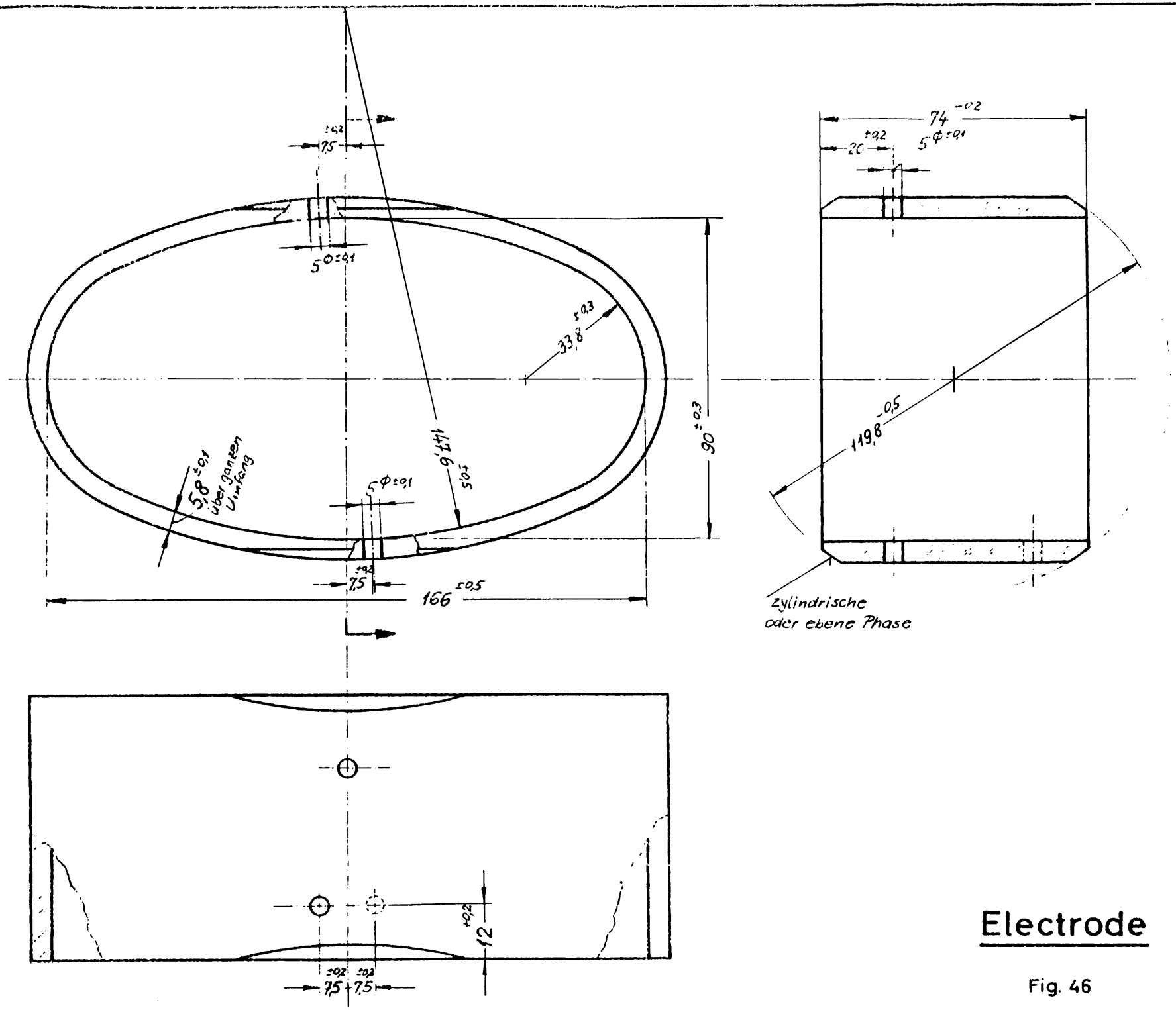

Electrode

Fig. 46

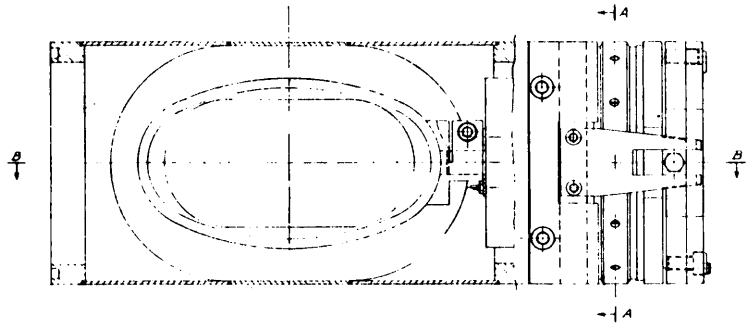

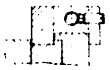

Coupe D-D

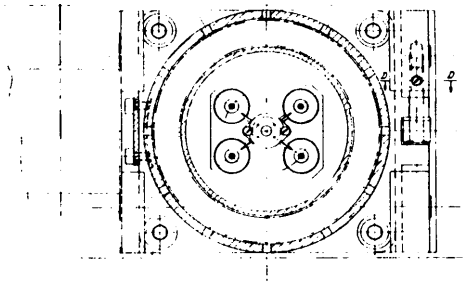

Coupe A-A

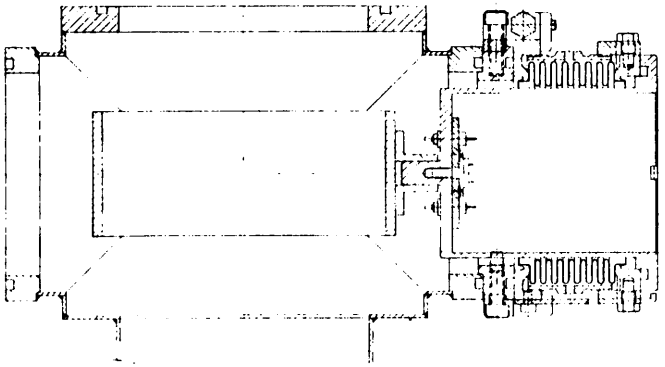

Coupe B-B

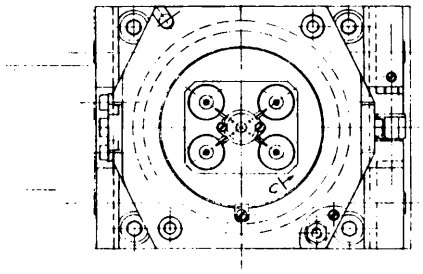

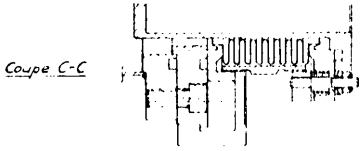

Coupe C-C

Pick – up station

Fig. 47

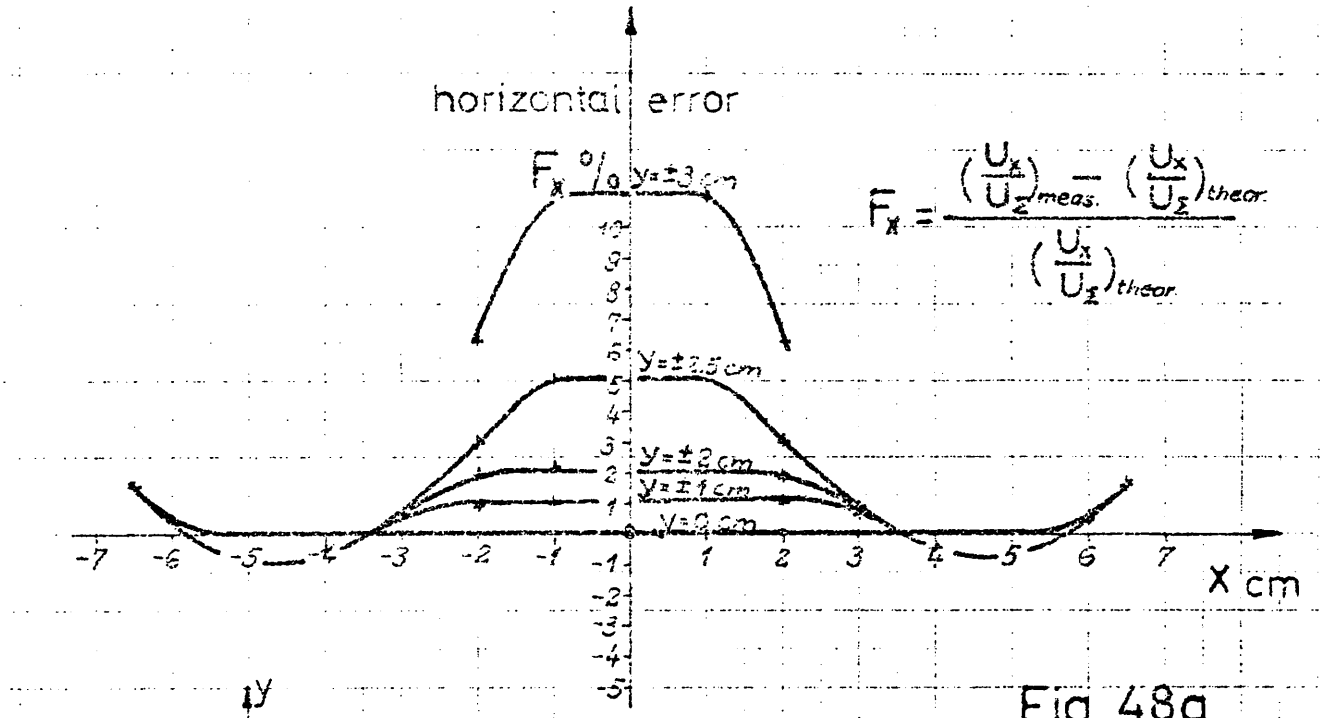

Fig. 48a

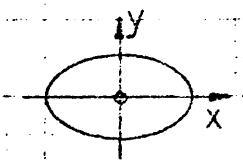

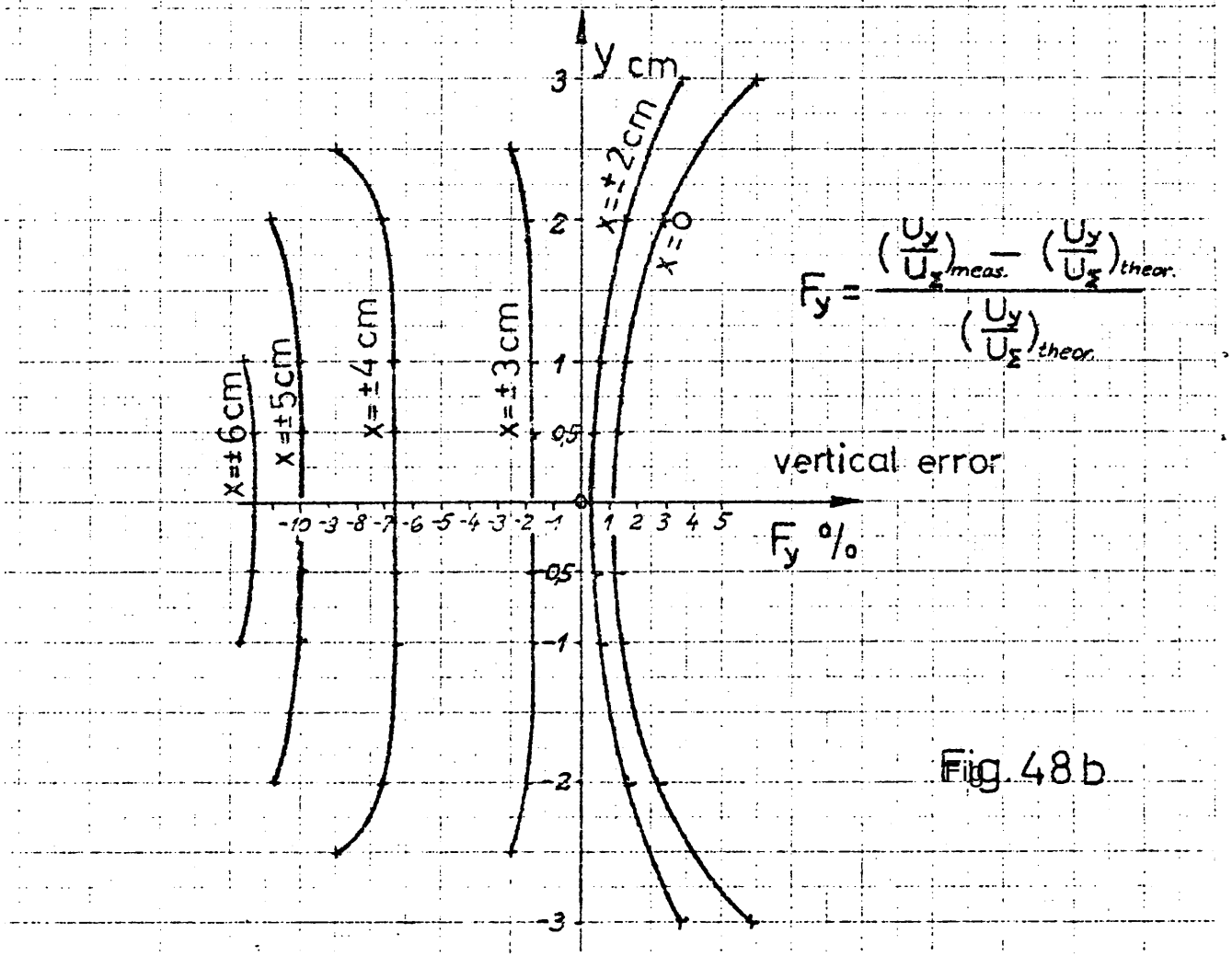

Fig. 48b

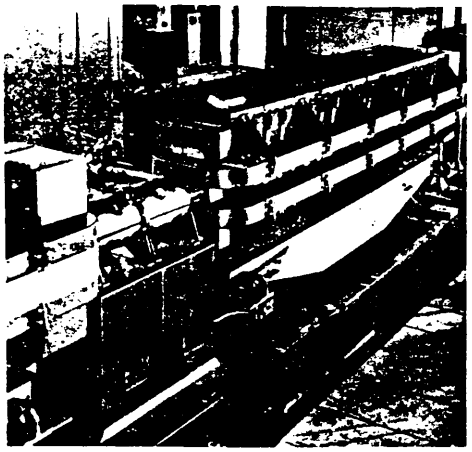

Photo 1

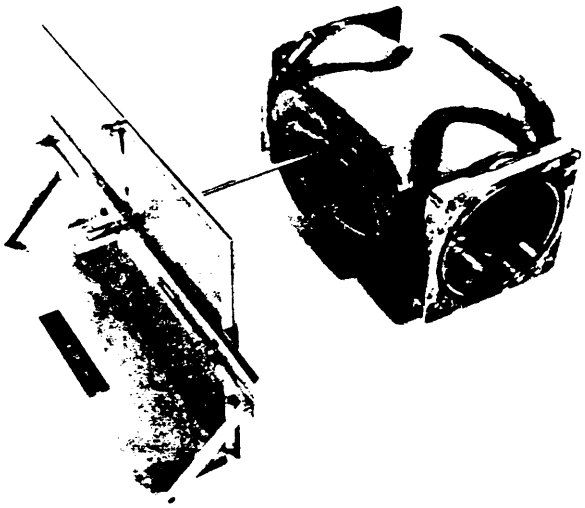

Photo 2

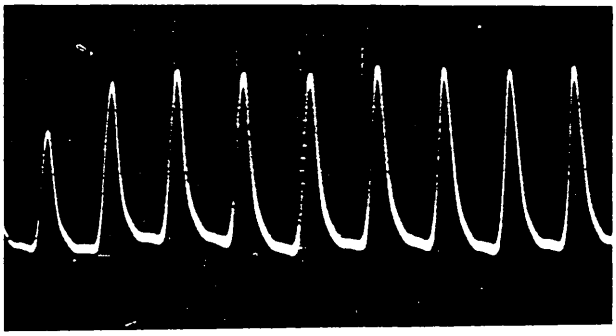

Photo 3
100 ns/cm

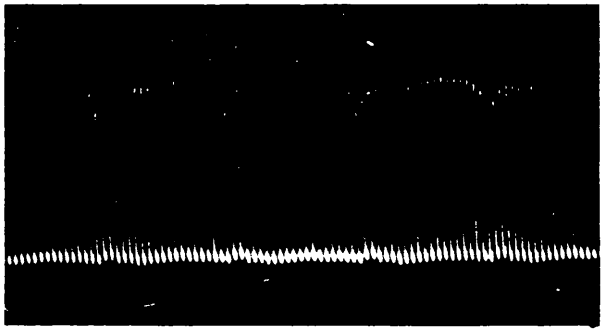

Photo 4
1 µs/cm

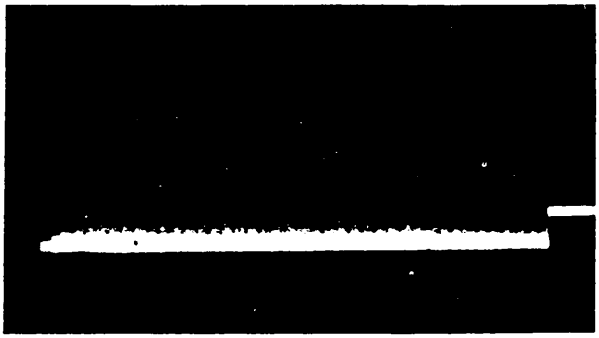

Photo 5
100 ms/cm

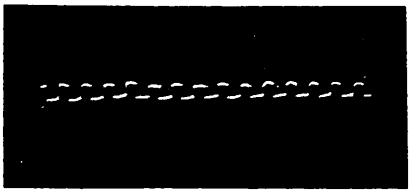

Photo 6
10/us/cm

Photo 7

Photo 8
vertical
transition

Photo 9
radial
transition

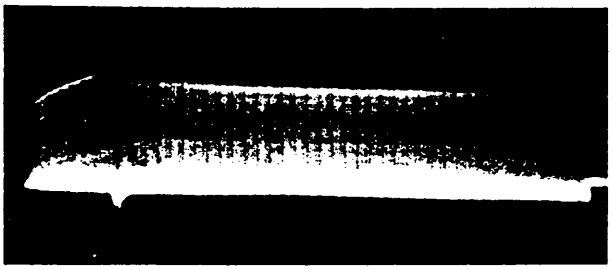

Photo 10
vertical
whole cycle

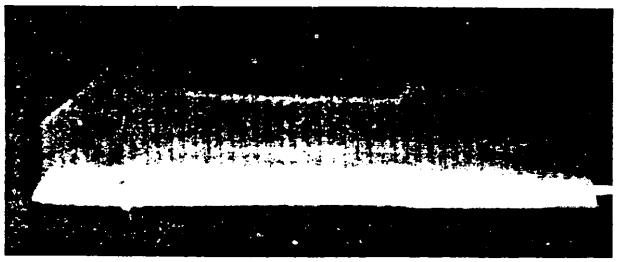

Photo 11
radial, whole cycle

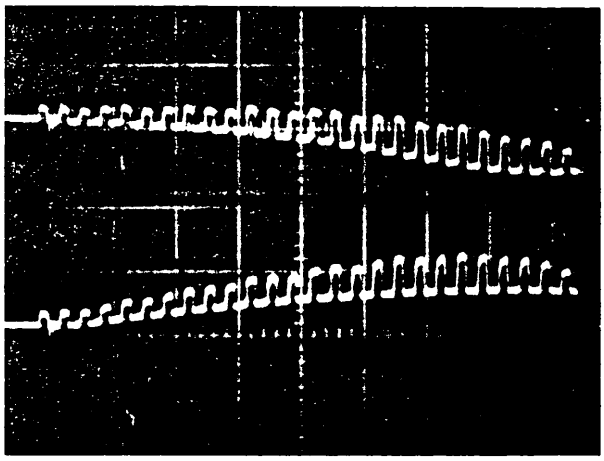

Photo 12
radial, 20/us/cm

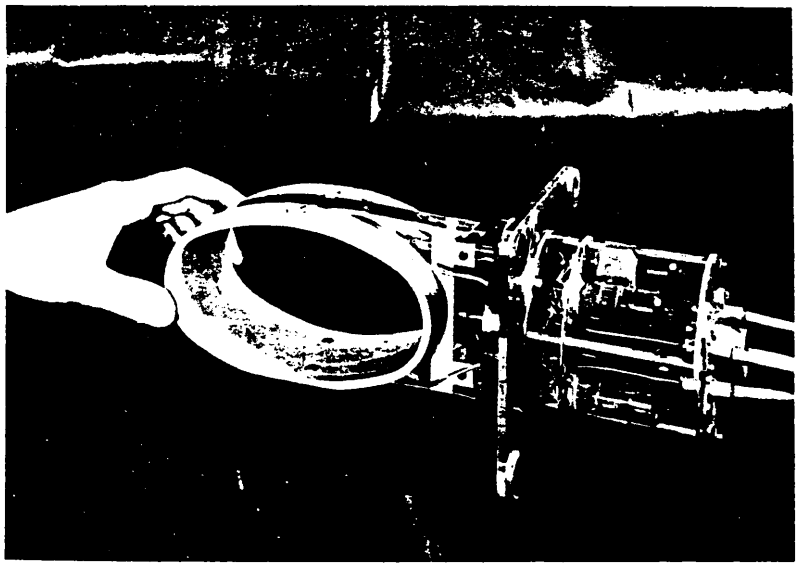

Photo 13

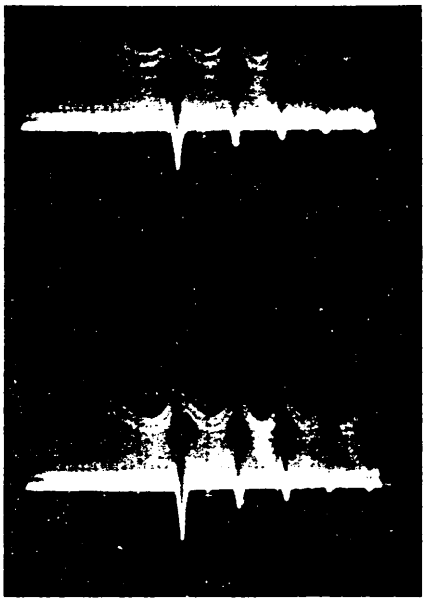

Photo 14

transition
2 ms/cm

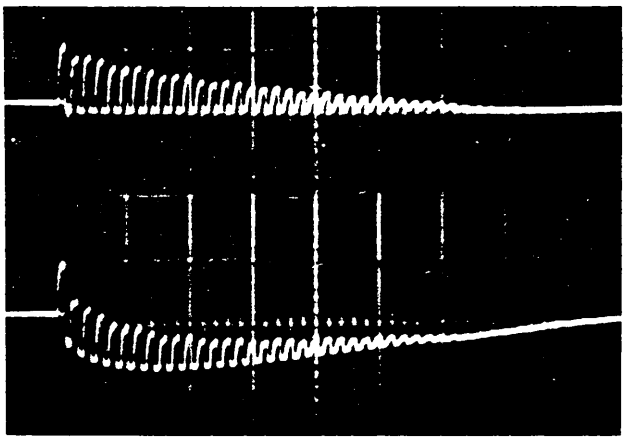

biased
-50 V

0 V

Photo 15

injection
radial ext.

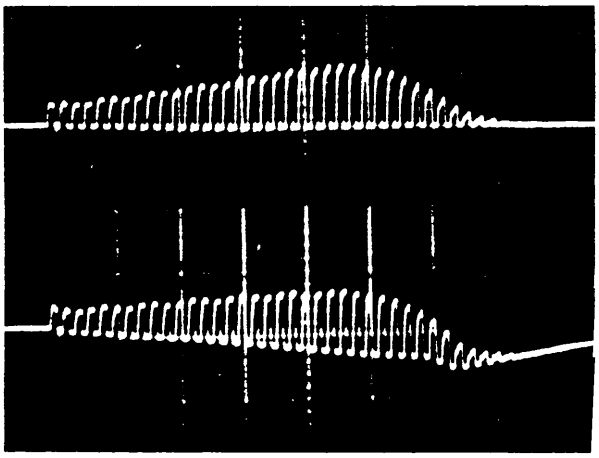

biased
-50 V

0 V

Photo 16

injection
radial int.

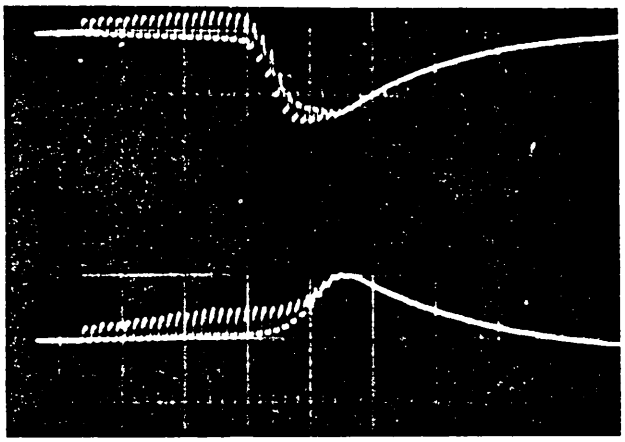

biased

0 V

-60 V

Photo 17

injection
radial int.
20/us/cm

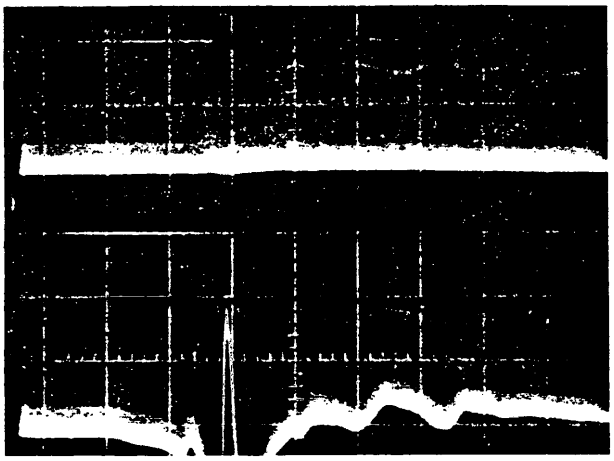

biased

-200 V

0 V

Photo 18

transition
radial int.
2 ms/cm

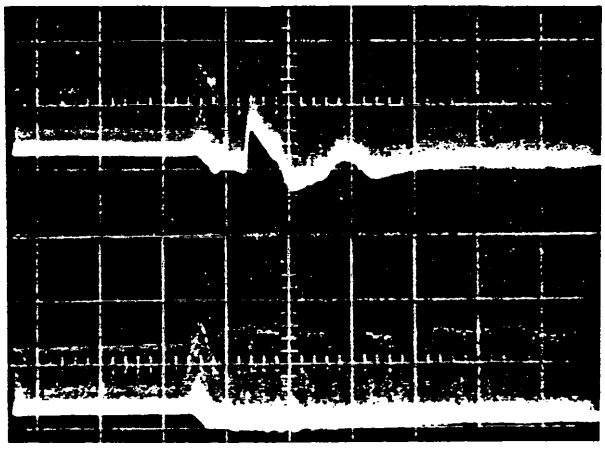

biased

0 V

-300 V

Photo 19

transition
radial ext.
2 ms/cm

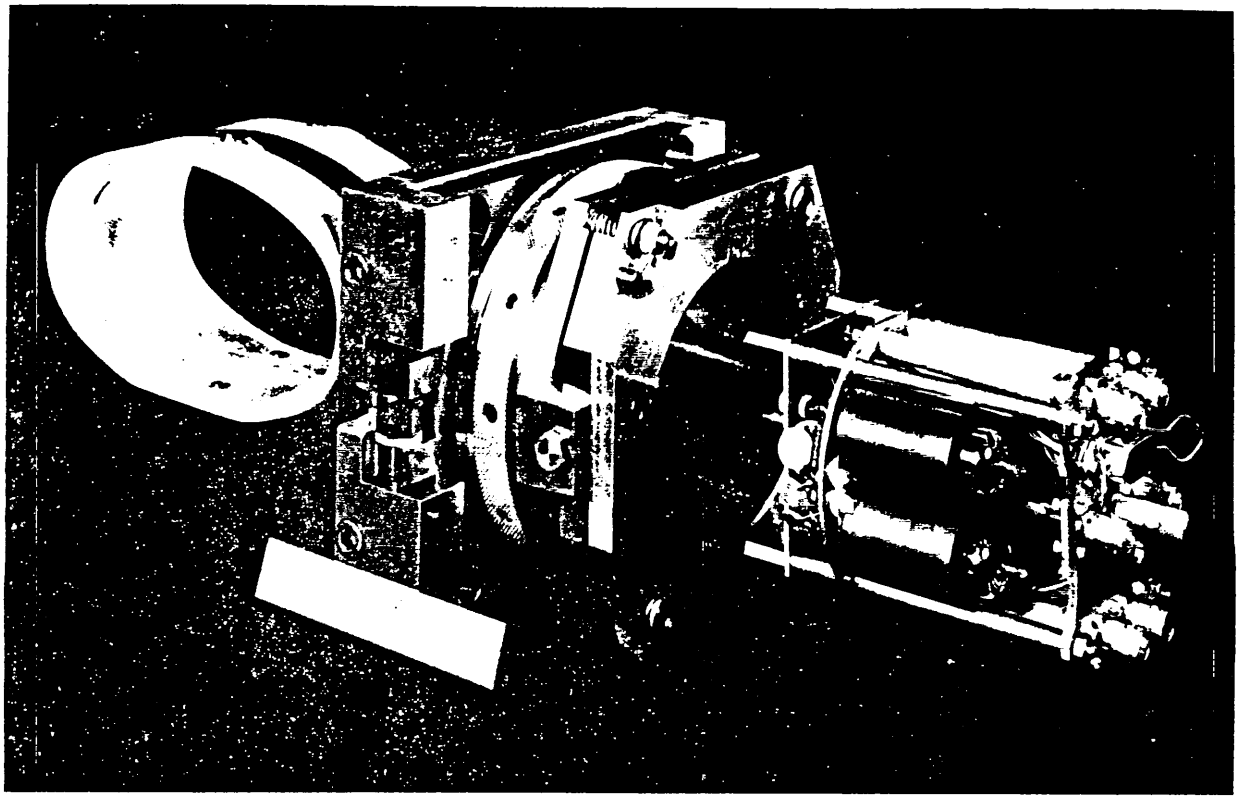

Photo 20

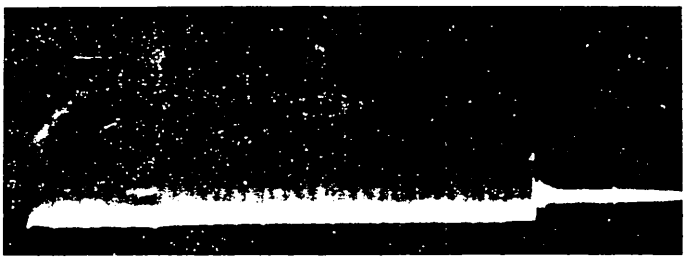

Photo 21

sum signal
whole cycle
0,1 s/cm

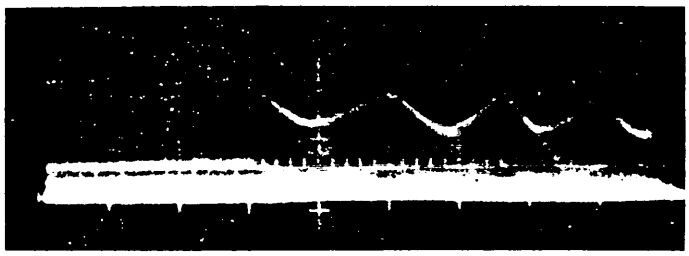

Photo 22

sum signal
transition
2 ms/cm

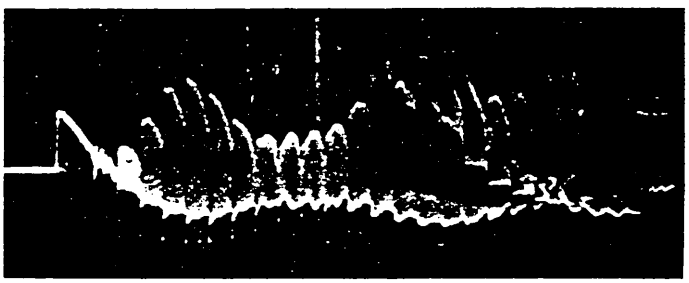

Photo 23

sum signal
injection
20 µs/cm